

# Chemistry and Physics of Complex Systems Facility

The Chemistry and Physics of Complex Systems (CPCS) Facility supports the U.S. Department of Energy (DOE) mission of fostering fundamental research in the natural sciences to provide the basis for new and improved energy technologies and for understanding and mitigating the environmental impacts of energy use and contaminant releases. This research provides a foundation for understanding interactions of atoms, molecules, and ions with materials and with photons and electrons. Particular emphasis is on interfacial processes.

A distinguishing feature of research at national laboratories is their approach to problem-solving. Significant scientific issues are addressed using focused and multidisciplinary investigative teams with each team member bringing a particular skill and capability to bear on the problem. This approach accelerates progress. The same approach—involving groups of scientists within the program as well as collaborators from throughout Pacific Northwest National Laboratory (PNNL) and the external scientific community—is inherent in how the CPCS Facility is managed.

The CPCS Facility and its staff have particular capabilities and expertise that support user research involving preparation and spectroscopic analysis of molecular clusters; high-resolution imaging of biological samples and studies of cellular processes, including DNA damage and repair and low-dose radiation processes; ultra-fast and non-linear optical spectroscopies; ultra-high-resolution spectroscopy for measurements of electronic and geometric structures and dynamics; surface and interface structure; chemical reaction dynamics and kinetics; ion-molecule traps and storage technology; and specialized chambers, instruments, and models for studying chemical reactivity and analyzing atmospheric species including aerosols.

Our research underpins the fundamental understanding of chemical transport and reactivity in the condensed phase. It addresses the underlying uncertainties in thermal and non-thermal (i.e., radiation) chemistry, interfacial molecular and ionic transport, and other processes in complex natural and human-made systems related to energy use, environmental remediation, waste management, and understanding biological responses to environmental stresses. One focus is on structures and processes of molecular and nanoscale systems in complex environments such as condensed phases and interfaces. Research guides the development of new materials and approaches for clean and efficient energy use.

## Instrumentation & Capabilities

- reaction mechanisms at solid, liquid, and gas interfaces
- high-energy processes at environmental interfaces
- cluster models of the condensed phase
- single-molecule spectroscopy and biomolecular sciences
- ultra-sensitive and environmental analysis.

Another central feature is the development of innovative experimental methods with broad applications to research in the natural sciences. Two examples of innovative methods developed in the CPCS Facility include 1) detecting and monitoring trace atmospheric species, including gaseous and particulate matter, and 2) studying biological processes important in the environment and health, including imaging of live cells to observe the reaction dynamics of functioning biological systems in realtime, advancing our understanding of protein-protein interactions and DNA damage and repair using single-molecule spectroscopy, and studying cellular responses to low-dose radiation using novel instrumentation.

## Capabilities

The capabilities of the CPCS Facility support research in five general areas, which are described below.

**Reaction Mechanisms at Solid, Liquid, and Gas Interfaces.** Research in this area focuses on developing fundamental molecular information about processes occurring at the interfaces between environmentally important liquids, solids, and gases. For example, a common element in environmental restoration is the need to understand molecular processes 1) in aqueous solutions and at the interface between aqueous and organic solutions and 2) at the interface between aqueous solutions and environmentally important solid materials. Examples of instruments that enable this research are shown in Figures 1 and 2.

Molecular processes occurring at liquid-liquid interfaces also play an important role in the subsurface transport of contaminants such as organic solvents (e.g., chlorinated hydrocarbons) released into soil and groundwater. Processes at the gas-liquid interface are critical in atmospheric transport processes.

Model systems such as amorphous solid water permit detailed studies of solvation and the effects of solvation on chemical reactivity. These studies provide information about intermolecular interactions that lay the foundation for accurate modeling of solution processes. Studies provide information about factors that control the rates of reactions in solution. This

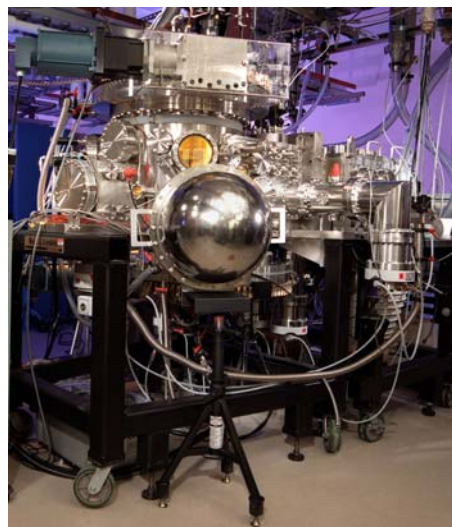


**Figure 1.** State-of-the-art molecular beam surface-scattering and kinetics instrument.



**Figure 2.** Combined instrument that allows fluorescent optical microscopes and magnetic resonance microscopes to focus on the same samples at the same time.

information is essential to both predicting the fate of contaminants in aqueous environments and influencing the selectivity of ligands for specific ions important in developing separations agents for waste treatment processes.

It is also crucial to understand molecular processes at the interface between aqueous solutions and environmentally important materials, such as aerosol particles, minerals, and glasses. This addresses fundamental science questions about contaminant fate and transport and waste immobilization. Because most environmental materials are in an oxidized form, we emphasize the structure and chemistry of oxide materials, especially naturally occurring oxides of silicon, aluminum, and iron. The adsorption of species on and their incorporation in soil minerals affect their transport through soil. Mineral interfaces can enhance or retard reactivity as well as transform contaminants. Knowledge of molecular processes at solid-liquid interfaces is also important to understanding the stability of glasses proposed for encapsulating high-level radioactive wastes that must be stored for long periods of time. Over the long half-lives of radionuclides, water can degrade these waste-encapsulating glasses, thus leading to higher-than-expected releases of radionuclides.

#### **High-Energy Processes at Environmental Interfaces.**

Research in this area focuses on obtaining a mechanistic understanding of chemical transformations resulting from electronic excitation in condensed-phase materials relevant to the DOE environmental cleanup mission. Examples of capabilities that enable this research are shown in Figures 3 and 4. Energetic processes are important in the degradation of mixed wastes because of the radiolytic decay-driven chemistry that occurs in the solid and liquid phases of stored radioactive waste and in final waste storage forms. Reactions occurring at interfaces are of particular interest for characterizing material composition and response to electronic excitation. We use pulsed femtosecond and nanosecond laser sources to study laser-solid interactions in a combined experimental and theoretical program. Our goal is to continue development of models for excited-state reactions by measuring ultra-fast dynamic processes and by demonstrating laser control of solid-state chemistry.

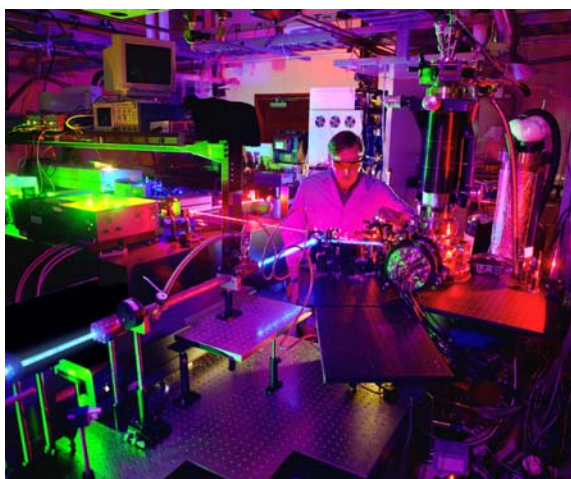


**Figure 3.** Laser desorption experiments investigate the effects of electronic excitation on crystalline materials.

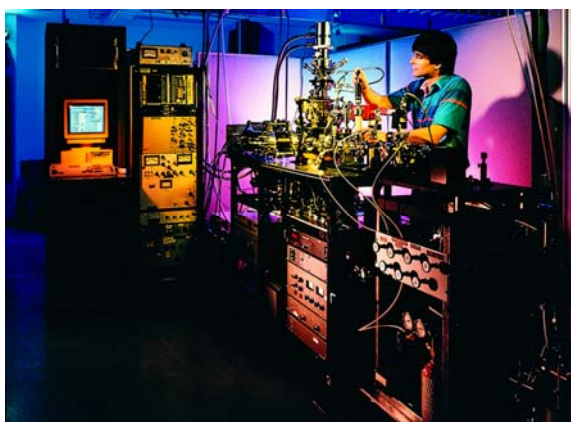


**Figure 4.** Electron-stimulated surface reaction apparatus is used to study non-thermal reactions that occur on surfaces or at interfaces.

### Cluster Models of the Condensed Phase.

This research is aimed at providing a molecular-level understanding of solvation and subsequent reactions in simple and complex systems as they relate to the chemistry of complex wastes, contaminated solids and groundwater, and other systems found in nature. A major experimental and theoretical effort is devoted to understanding surface and interface properties using cluster models to study structure and bonding. Small and controllable cluster systems provide atomic-level models that enable us to understand bulk surfaces and defect sites. They are also an excellent testing ground to benchmark theories intended for large and real-world systems. A productive collaboration in this area is illustrated in Figure 5.

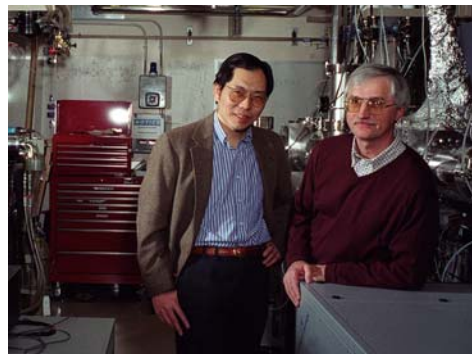


**Figure 5.** CPCS Facility users/collaborators Lai-Sheng Wang, Washington State University, Richland, Washington, and Alex Boldyrev, Utah State University, Logan, Utah, are combining experimental and theoretical approaches to understand the unique properties and characteristics of metal clusters. Their research is at the forefront of cluster science.

### Single-Molecule Spectroscopy and

**Biomolecular Sciences.** This research emphasizes single-molecule spectroscopy and high-resolution biological imaging techniques for studying biological systems. Recent advances in fluorescence microscopy, at both the W.R. Wiley Environmental Molecular Sciences Laboratory (EMSL) and elsewhere, make it possible to detect single molecules at room temperature and to conduct spectroscopic measurements to monitor their dynamic processes. We have demonstrated fluorescence imaging of single molecules by two-photon excitation with a femtosecond laser. This approach has several advantages—the excitation volume is small, the penetration is deep, and photo-damage is reduced for biological samples—thus offering the opportunity of viewing chemical reactions in a living cell in real time. Structures are known for many proteins that perform vital cell functions, including DNA damage repair, reaction catalysis, and cell signaling. Nanoscale-structure materials will affect their properties; Figure 6 provides an example. However, how they perform these functions is generally not understood. Single-molecule and single-cell measurements provide real-time data on the molecular motions involved during these functions and how the timing of these reactions is correlated with other cellular biological activities. These data are likely to produce new information that is otherwise hidden, and will open up exciting possibilities for probing cellular processes.

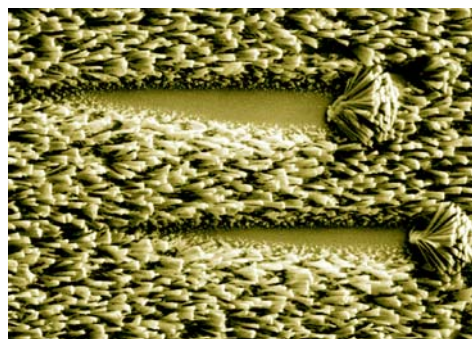


**Figure 6.** Nanostructures could be used to control and enhance chemical reactivity. Researchers at the CPCS Facility are trying to determine how molecules enter pores, are captured, and eventually released.

Another research area was that of cellular response to low-dose radiation at levels below standard detection limits. A novel spatially resolved cell irradiator allows the selective irradiation of individual cells to reveal the

individual pathways that lead to radio-adaptive responses. Information obtained from use of this instrument enables researchers to understand the biological consequences and health effects associated with very low radiation doses. Such knowledge can help form more technically rigorous bases for understanding human health and environmental protection standards. Near the end of 2004, the low-linear-energy-transfer microbeam used in this low-dose research was relocated to the University of Maryland School of Medicine (UM), where it is now fully operating. UM has several unique biological assay systems available that will use the microbeam.

**Ultra-Sensitive and Environmental Analysis.** Research in this area focuses on developing a suite of instrumentation for fast, accurate, highly sensitive, and discriminatory real-time analyses of chemical and biological natural or human-made agents. Such instruments are ideally suited for identifying and quantifying many gases and pollutants, trace isotopic species, metabolic products in the breath, and chemical precursors and products from industrial processes. Some of these techniques can be developed for remote probing over long optical paths for remote interrogation of trace absorption features. Our infrared methods are supported by a state-of-the-art, high-resolution infrared spectroscopy laboratory, that also is used for studies of the structures and dynamics of molecular species important in contaminant chemistry, photochemistry, and atmospheric processes. The high-resolution infrared spectroscopy laboratory is shown in Figure 7.



**Figure 7.** The high-resolution infrared spectroscopy laboratory is used by numerous users and U.S. government agencies to obtain high-resolution infrared spectra for applications in remote sensing, atmospheric science, space and planetary research, and infrared databases.

Characterization of particulate matter in the atmosphere represents a unique challenge. Several approaches are employed that, in combination, are designed to understand the evolving inventory of atmospheric particulate matter and how particulates are changed by reactions with gas-phase species, photochemistry, and condensation and evaporation processes. One approach uses new mass spectrometric techniques for aerosol analysis. This instrumentation is built around a laser desorption/ionization mass spectrometer with an asymmetric ion trap for simultaneous positive/negative ion detection. It provides real-time sampling and analysis of aerosol particles in a field-deployable unit that is more compact and less expensive than current instruments.

In conjunction with this instrumentation, new devices are being developed and deployed to collect and preserve field samples for future automated analysis of individual particles in the laboratory. These same samples enable characterization of the chemical reactivity of native aerosols that can be used for comparison in laboratory studies of the formation and reactivity of model aerosol species. These studies are complemented by fundamental studies of the gas-phase chemistry of aerosol precursor molecules.

## Upgrades

### Photo-Emission Electron Microscope.

In November 2004, a new photo-emission electron microscope (PEEM), shown in Figure 8, was installed in the Energetic Processes Laboratory (EPL) in EMSL. The PEEM is capable of imaging nanoscale surface structures by imaging electron emission induced by ultraviolet and laser light sources. The PEEM will be applied to surface science studies of individual nanostructures and catalytic sites on specially designed metal, semi-conducting, and metal oxide substrates.

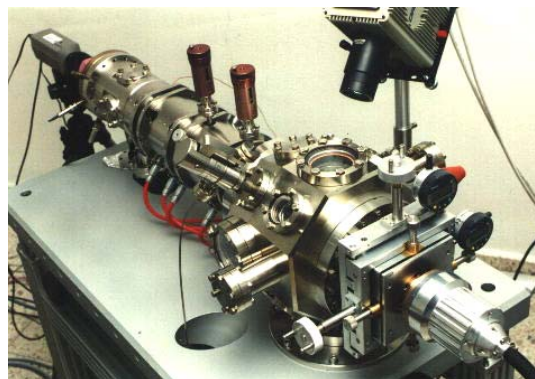


Figure 8. Photo-emission electron microscope.

Because these sites are of nanometer dimension, we selected the highest resolution PEEM available from the manufacturer, Elmitec. The Elmitec PEEM uses inherently low-aberration magnetic lens elements to achieve the highest theoretical and practical resolution. The new PEEM instrument will be combined with the ultrafast laser sources in EPL to study femtosecond dynamical processes with unprecedented spatial resolution.

**High-Resolution Fourier Transform Spectrometer.** A Bruker 125-HR Fourier transform spectrometer was installed in the High-Resolution Infrared Spectroscopy Laboratory in August 2004. This spectrometer has been custom configured for an ultimate spectral resolution of  $0.0012\text{ cm}^{-1}$  and can cover the  $10\text{ to }45,000\text{ cm}^{-1}$  spectral region. The completely redesigned spectrometer boasts all digital electronics, with each detector having its own analog digital converter, for improved performance. The spectrometer can be interfaced to a host of accessories for handling gas, liquid, and solid samples.

## Future Directions

In 2005, the CPCS Facility will focus on accomplishing high-impact science and expanded instrument capability development that supports research related to chemical transport and reactivity in the condensed phase, molecular processes, aerosol characterization, and biological imaging. Research will also support the PNNL Biogeochemistry Grand Challenge and the W.R. Wiley Environmental Molecular Sciences Laboratory (EMSL) Grand Challenge in membrane biology.

The CPCS Facility staff will continue to build visibility of the facility and of EMSL capabilities through:

- journal publications
- state-of-the-art instrument development and creation of innovative experimental methods
- fundamental multidisciplinary research collaborations with distinguished scientists
- presentations at national meetings
- service to professional societies and government agencies.

## Correlated Topographic and Spectroscopic Imaging by Combined Atomic Force Microscopy and Optical Microscopy

*D Hu,<sup>(a)</sup> M Miodrag,<sup>(a)</sup> NA Klymyshyn,<sup>(a)</sup> YD Suh,<sup>(a)</sup> and HP Lu<sup>(a)</sup>*

*(a) Pacific Northwest National Laboratory, Richland, Washington*

*Optical microscopy has been in development for hundreds of years. Improving the contrast and resolution for biological applications has been a major endeavor.*

Many techniques have been tried to improve contrast in optical microscopy, including the use of fluorescence and Raman imaging. Introducing fluorescent labels to a sample allows a species to be imaged with high sensitivity and high contrast. Recently, fluorescence lifetime imaging microscopy (FLIM) was found to further improve contrast by exploiting the lifetime difference of the fluorescent species and the local environments.

Raman near-field scanning microscopy is a powerful approach to obtaining topographic and spectroscopic characterization data simultaneously for imaging biological and nanoscale systems. To achieve optical imaging at high-spatial resolution beyond the diffraction limit, apertureless metallic scanning tips were used to enhance the laser illumination local electromagnetic field at the apex of the scanning tips. We recently published our work on combined fluorescence imaging with atomic force microscope (AFM)-metallic tip enhancement, finite element method simulation of tip enhancement and their applications on AFM-tip-enhanced fluorescence lifetime imaging (AFM-FLIM), and correlated AFM and FLIM imaging of living cells (Hu et al. 2004).

We used the frequency-domain finite element method (FEM) to characterize the near-field electromagnetic field distribution at the metallic-coated AFM-tip apex by solving classical Maxwell's equations in the short-field approximation. FEM is a well established and reliable computational approach in electrical engineering research for simulating electromagnetic fields. An example of these simulations is shown in Figure 1. Comparison of the simulation with an image of an actual tip is shown in Figure 1(C).

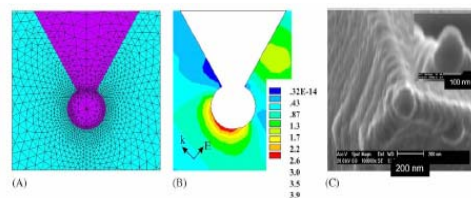


**Figure 1.** Three-dimensional FEM simulation of electromagnetic field distribution in the vicinity of the coated tip structure. (A) Cross section through the detail of finite element mesh. The geometry of the model is taken directly from the electron micrography measurements. The zoom-in mesh structure at the tip is shown in a two-dimensional plot. (B) Near-field distribution of the electromagnetic field in the vicinity of the gold-coated AFM-tip apex. Vectors  $K$  and  $E$  represent the laser-beam propagation vector and the electromagnetic field vector, respectively. (C) Field emission scanning electron micrography of the gold-coated AFM-tip. A globular gold structure at the apex of the tip is evident.

Using the above described tip, we performed simultaneous correlated topographic and spectroscopic imaging of fluorescent polymer nanoparticles beyond the diffraction-limited spatial resolution. Sample-scanning confocal fluorescence imaging of the sample slide was first performed to locate the fluorescent nanospheres. Then, the same sample area was imaged by tip-scanning tapping-mode AFM with gold-coated tips. Figures 2(A) and 2(B) are correlated fluorescence intensity and AFM topographic images from the same sample area. Figure 2(A) shows a confocal fluorescence image of a nanosphere sample on a glass coverslip. The nanospheres appear as a bright spot at a spatial resolution at about the diffraction limit (approximately 300 nm).

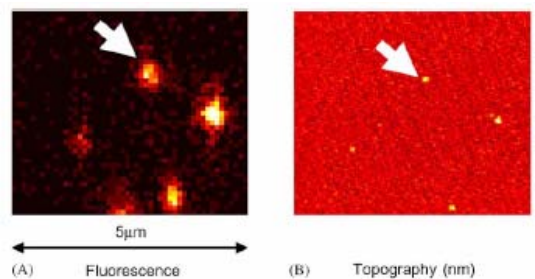


**Figure 2.** The fluorescence intensity image (A) and AFM image (B) of the same sample area containing 40-nm fluorescence nanospheres. The sample was first imaged by sample-scanning confocal fluorescence microscopy and then by tip-scanning AFM of the same area.

We also explored the utility of correlated AFM/FLIM imaging on *Shewanella oneidensis* MR-1 cells expressing the MCP-YFP fusion. Because the sizes of the bacterial cells are typically around 1 µm, which is very small for far-field optical imaging, the high-resolution imaging of AFM is important for investigating the subcellular structure of bacteria. The correlated AFM height image, fluorescence intensity image, and fluorescence lifetime image of a single cell are shown in Figures 3(A) through 3(C), respectively.

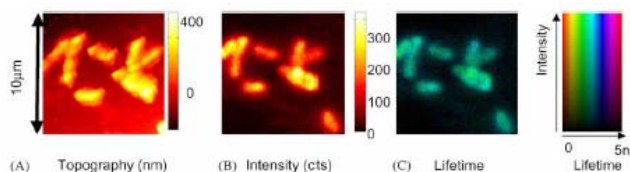


**Figure 3.** Composite correlated AFM-confocal FLIM image of *S. oneidensis* bacterial cells on polylysine surface: (A) topographic image, (B) confocal fluorescence intensity, and (C) confocal fluorescence lifetime image.

Based on near-field metallic-tip-enhanced microscopy and FEM simulation, we developed and applied a combined approach using AFM and optical microscopy to investigate the correlated topographic and spectroscopic information of nanoparticle and biological systems. Metallic AFM-tip enhancement enabled us to obtain optical images with spatial resolution beyond the diffraction limit. Correlated topography, fluorescence intensity, and fluorescence lifetime images of living cells show high promise of biological optical imaging beyond the diffraction limit, providing information not obtainable using noncorrelated and far-field imaging approaches.

## Reference

Hu D, M Micic, N Klymyshyn, YD Suh, and HP Lu. 2004. "Correlated Topographic and Spectroscopic Imaging by Combined Atomic Force Microscopy and Optical Microscopy." *Journal of Luminescence* 107(1-4):4-12.

## Single-Molecule Protein-Protein Interaction Dynamics in Cell Signaling

X Tan,<sup>(a)</sup> P Nalbant,<sup>(b)</sup> A Toutchkine,<sup>(b)</sup> D Hu,<sup>(a)</sup> ER Vorpapel,<sup>(a)</sup> KM Hahn,<sup>(b)</sup> and HP Lu<sup>(a)</sup>

(a) Pacific Northwest National Laboratory, Richland, Washington

(b) The Scripps Research Institute, La Jolla, California

*Protein-protein interactions play critical roles in intracellular signaling within biological systems, acting as molecular-level switches in signaling pathways to regulate cellular response to stimuli. These interactions often involve complex mechanisms and inhomogeneous dynamics.*

Cell-signaling processes are often initiated through amplification of a few copies of protein-interaction complexes along the signaling pathway. Protein interactions in living cells are typically inhomogeneous, both spatially and temporally, and protein interaction dynamics can be different from molecule to molecule and from site to site. Furthermore, the dynamics can be different from time to time for the same individual molecules, which is beyond the scope of the conventional kinetics. Single-molecule spectroscopy is a powerful and complementary approach that can be used to decipher such spatially and temporally inhomogeneous protein interaction systems, providing new information not obtainable from static structure analyses, thermo-dynamics characterization, and ensemble-averaged measurements.

We have applied single-molecule spectroscopy to study the interactions of an intracellular-signaling protein Cdc42, a guanosine 5'-triphosphate (GTP)-binding protein, with its downstream effector protein, Wiskott-Aldrich Syndrome Protein (Tan et al. 2004) (Figure 1). In this work, a Wiskott-Aldrich Syndrome Protein fragment that binds only the activated Cdc42 was labeled with a solvatochromic dye to probe the hydrophobic interactions at the protein-protein interface that are significant to

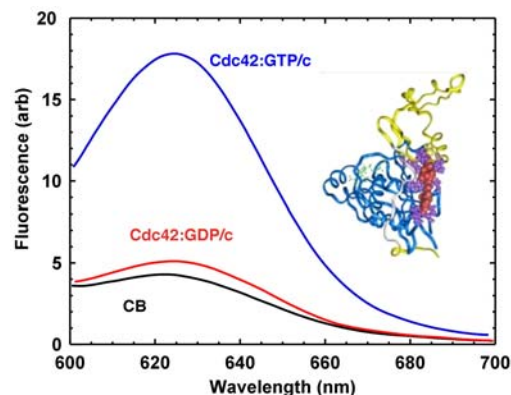


**Figure 1.** Protein-protein interaction fluorescence assay and fluorescence characterization of the I-SO dye probe. Ensemble fluorescence assays of Cdc42 with a  $\beta$ -catenin destruction (CBD) biosensor using fluorescence spectral measurements. Fluorescence spectra were obtained with excitation at 568 nm. The blue curve represents the active GTP-activated Cdc42-forming complexes with dye-labeled CBD; the red curve represents the GDP-loaded Cdc42 with dye-labeled CBD; and the black curve represents the dye-labeled CBD alone. A non-hydrolyzable GTP analogue, GTP- $\gamma$ -S, was used to lock Cdc42 in the active conformation. Thus, the GTP binding and unbinding process was eliminated from the single-molecule experiments that measured only the activated Cdc42 interacting with CBD. The effects of GTP- $\gamma$ -S are the same as that of GTP, and the biological relevance and validity of using GTP- $\gamma$ -S has been well established in literature. Inset: A structure based on molecular dynamics calculations of protein complex Cdc42 (dark ribbon structure on the left)/Wiskott-Aldrich Syndrome Protein (light ribbon structure on the right) with dye attachment (dark ball structure) outside the Cdc42/Rac-interactive binding motif among hydrophobic residues (purple).

Cdc42/Wiskott-Aldrich Syndrome Protein signaling recognition. Cdc42 is a monomeric GTP-binding protein (a GTPase) that acts as a molecular switch in signaling pathways to regulate various cellular responses. Cdc42 GTPase can be activated by binding to GTP, and the activated Cdc42 then binds and activates a series of effector proteins via direct protein-protein interactions.

Our single-molecule spectroscopy study revealed static and dynamic inhomogeneous conformational fluctuations of the protein complex involving bound and loosely bound states of the protein-protein interaction complex (Tan et al. 2004).

Using single-molecule photon stamping detection, we were able to record single-molecule fluorescence images (Figure 2), intensity trajectories, and nanosecond fluorescence lifetimes simultaneously (Tan et al. 2004; Hu and Lu 2003). From the trajectories of single protein complexes,  $\{I(t)\}$ , we observed a more than threefold variation in fluorescence intensity fluctuations at a timescale ranging over two orders of magnitude. Based on the control experiments, which indicated that the detectable single-molecule fluorescence comes only from the Cdc42- CBD complex, we attributed the fluorescence intensity fluctuations to conformational fluctuations of the protein complex (Tan et al. 2004). The autocorrelation function,  $C(t) = \langle \Delta I(t)\Delta I(0) \rangle / \langle \Delta I(0)^2 \rangle$ , is calculated from a single-complex fluorescence intensity trajectory  $I(t)$ , where  $\Delta I(t) = I(t) - \langle I(t) \rangle$ . Figure 3A shows an example of the autocorrelation function of a single-complex intensity trajectory. A typical spike at  $t = 0$  is caused by uncorrelated measurement noise and faster fluctuations beyond the instrument time-resolution. For  $t > 0$ , the autocorrelation function can be fit to a biexponential decay  $C(t) = A_f \exp(-k_f t) + A_s \exp(-k_s t)$ , with  $A_f = 0.17$ ,  $k_f = 250 \pm 60 \text{ s}^{-1}$  and  $A_s = 0.14$ ,  $k_s = 45 \pm 10 \text{ s}^{-1}$ . The autocorrelation functions of all single-complex trajectories are fit to either single-exponential or biexponential decays.

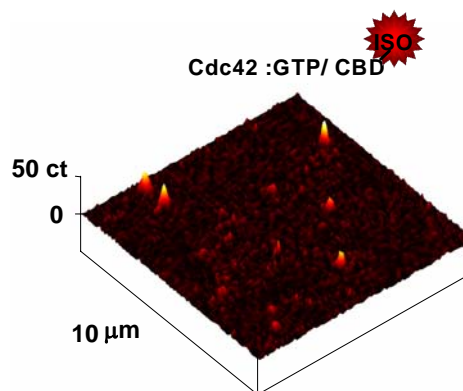


**Figure 2.** Single-molecule spectroscopy and imaging study of Cdc42-CBD binding dynamics. A single-molecule fluorescence raster-scanning image of GTP-loaded Cdc42 in complex with dye-labeled CBD biosensor.

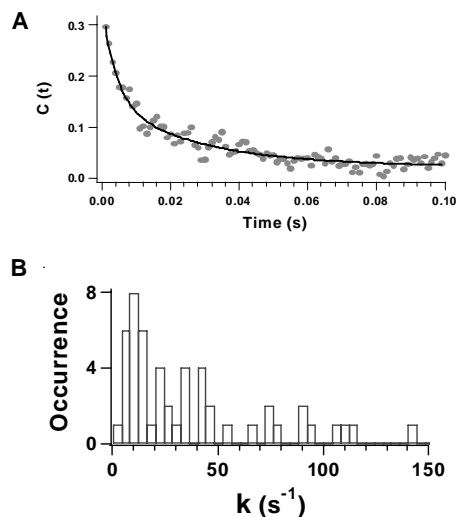


**Figure 3.** A) The second-order autocorrelation function,  $C(t)$ , calculated from a fluorescence intensity trajectory  $I(t)$  of a single Cdc42-CBD complex. The solid curve is a bi-exponential fit with decay rates of  $250 \pm 60$  and  $45 \pm 10 \text{ s}^{-1}$ . B) The occurrence histogram of the single-complex Cdc42-CBD conformational fluctuation rates is constructed by using parameters from fitting the autocorrelation functions for 60 individual protein complexes.

Detailed experimental characterizations of the protein-protein interaction conformational fluctuation concluded that the dynamics of the conformational fluctuations involve bound and loosely bound states of the protein complex. The loosely bound states are a subset of conformations with deviated nuclear displacements from the bound equilibrium states; they distort the protein-protein interaction interface and the local environment of the dye probe without disrupting the sub-nanometer long-range interactions so that the overall protein complex is still associated. Compared with the bound state, the loosely bound state gives significantly lower fluorescence intensity, as the distorted protein-protein interaction interface probed by solvatochromic dye becomes more solvent-accessible and hydrophilic. With respect to the ensemble-averaged assay experiment (Figure 1), the bound state corresponds to the high emission-intensity Cdc42-CBD bound equilibrium state, where the local environment of the dye probe is more hydrophobic, and the loosely bound state has a hydrophilic local environment of the dye probe resembling the environment of CBD alone. In the measured single-molecule experiments, fluorescence fluctuations at millisecond and subsecond timescales reflect the Cdc42-CBD conformational changes between the bound and loosely bound states.

One of the most interesting observations is that the conformational fluctuation rates are found to be highly inhomogeneous (Figure 3B), which is reflected by a broad distribution of fluctuation rates. Variations of more than two orders of magnitude occur in the conformational fluctuation rates among individual protein complexes. Although it is difficult to identify exactly how many conformational states contribute to the inhomogeneous distribution, at least two sub-groups of states are associated with conformational fluctuations at approximately 10/sec and 40/sec (Figure 3B). About 25% of the single-complex fluorescence intensity trajectories demonstrated biexponential decays, indicating non-Poisson kinetics. The non-Poisson behavior suggests that the Cdc42-CBD interactions have both static and dynamic inhomogeneities.

## References

Hu D and HP Lu. 2003. "Single-Molecule Nanosecond Anisotropy Dynamics of Tethered Protein Motions." *Journal of Physical Chemistry B* 107(2):618-626.

Tan X, P Nalbant, A Touthkine, D Hu, ER Vorpapel, KM Hahn, and HP Lu. 2004. "Single-Molecule Study of Protein-Protein Interaction Dynamics in a Cell Signaling System." *Journal of Physical Chemistry B* 108(2):737-744.

## Boron Clusters: It's a Planar World

HJ Zhai,<sup>(a)</sup> B Kiran,<sup>(a)</sup> J Li,<sup>(a)</sup> AN Alexandrova,<sup>(b)</sup> AI Boldyrev,<sup>(b)</sup> and LS Wang<sup>(a)</sup>

(a) Washington State University Tri-Cities, Richland, Washington

(b) Utah State University, Logan, Utah

One of the most interesting features of elemental boron and many bimetallic boron compounds is the occurrence of highly symmetric icosahedral boron clusters. The rich chemistry of boron is also dominated by three-dimensional cage structures. Despite its proximity to carbon in the periodic table, elemental boron clusters have been scarcely studied experimentally, and their structures and chemical bonding have not been fully elucidated. Armed with new innovative experimental data and theories, chemists are becoming fascinated with the prospects for new families of functional boron clusters. Potential applications for such boron compounds includes their use in electronics, catalysis, and diagnostic/therapeutic medicine.

In a series of studies combining experimental studies using photoelectron spectroscopy and *ab initio* calculations, we have completely elucidated the structure and chemical bonding of small boron clusters (Zhai et al. 2003a, b). We confirmed that small boron clusters indeed prefer planar structures (Figure 1) and exhibit aromaticity and antiaromaticity according to the Hückel rules, akin to planar hydrocarbons. Aromatic boron clusters possess more circular shapes, whereas antiaromatic boron clusters are elongated, analogous to structural distortions of antiaromatic hydrocarbons. The planar boron clusters are thus the only series of molecules other than the hydrocarbons to exhibit size-dependent aromatic and antiaromatic behaviors, and these structures represent a surprising new dimension of the expanding chemistry of boron. A paper published in early 2004 describes this work (Ritter 2004).

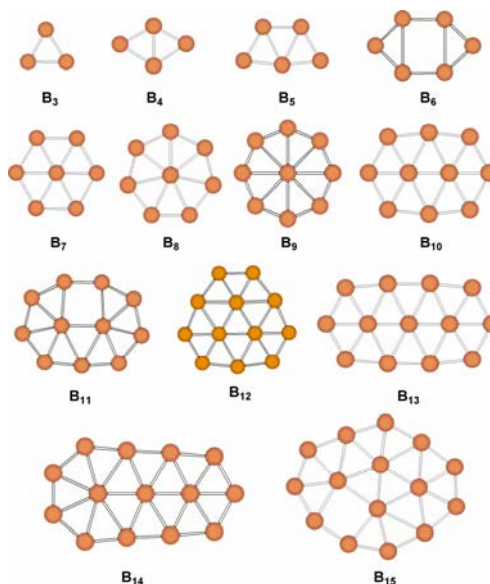


**Figure 1.** The computed structure of small planar boron clusters.

### References

Ritter SK. 2004. "Boron Flat Out." *Chemical and Engineering News* 82(9):28-32.

Zhai HJ, AN Alexandrova, KA Birch, AI Boldyrev, and LS Wang. 2003a. "Hepta- and Octacoordinated Boron in Molecular Wheels of 8- and 9-Atom Boron Clusters: Observation and Confirmation." *Angewandte Chemie International Edition* 42(48):6004-6008.

Zhai HJ, B Kiran, J Li, and LS Wang. 2003b. "Hydrocarbon Analogs of Boron Clusters: Planarity, Aromaticity, and Antiaromaticity." *Nature Materials* 2(12):827-833.

## Determination of Surface Exciton Energies by Velocity Resolved Atomic Desorption

WP Hess,<sup>(a)</sup> AG Joly,<sup>(a)</sup> KM Beck,<sup>(b)</sup> PV Sushko,<sup>(c)</sup> and AL Shluger<sup>(c)</sup>

(a) Pacific Northwest National Laboratory, Richland, Washington

(b) W.R. Wiley Environmental Molecular Sciences Laboratory, Richland, Washington

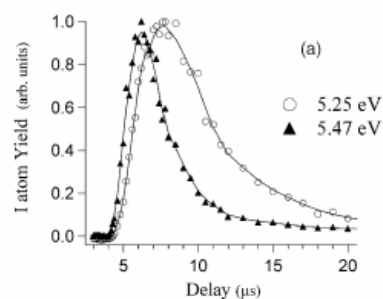
(c) University College, London, United Kingdom

*Selective electronic excitation of particular surface features, such as terraces, steps, and low coordinated sites, can induce reactions of the surface itself and of adsorbed molecules. Surface excitation may create both electron-hole pairs and surface excitons, which play a significant role in surface reactions and photo-catalysis. This can lead to advances in microelectronics, photo-catalysis, and particle beams of controlled energies and penetration.*

Electronic excitation of alkali halide surfaces leads to halogen- and alkali-atom desorption. Under ultraviolet irradiation, halogen atoms desorb from alkali halide crystals in densities sufficient to be used as an intense halogen atom source. Surface excitons are intimately involved in the halogen-atom desorption mechanism.

We have recently described a new spectroscopic method for probing surface exciton energies based on atomic desorption induced by tunable laser excitation. This ultrasensitive method, which we call surface electronic spectra detected by atomic desorption (SESDAD), allowed us to measure a sharp maximum in desorption yield of hyperthermal iodine atoms from KI where surface excitons had not previously been detected spectroscopically. Based on the good agreement between theory and experiment, we suggested that the photon energy corresponding to the maximum desorption yield should be very close to the surface exciton energy. This particle-detected spectroscopic feature, which represents the signature of the KI surface exciton, is clearly distinct and shifted to lower energy from the bulk exciton absorption band.

Those results demonstrated that surface electronic structure can be probed through detection of particle emission that occurs following photoexcitation. However, SESDAD requires stable tunable laser sources, and for some especially wide-gap materials, may even require use of synchrotron facilities. In this paper, we describe a much simpler method for determining surface exciton band energies of alkali halides based on velocity-resolved atomic desorption (VRAD) (Hess et al. 2004). VRAD requires only point-tunable pulses that may be generated using common table-top laser systems. Based on the surface exciton model of hyperthermal halogen desorption from alkali halides, we show that a simple analysis of the kinetic energy distribution of photo-desorbed surface atoms can be used to predict the surface exciton band center energies.



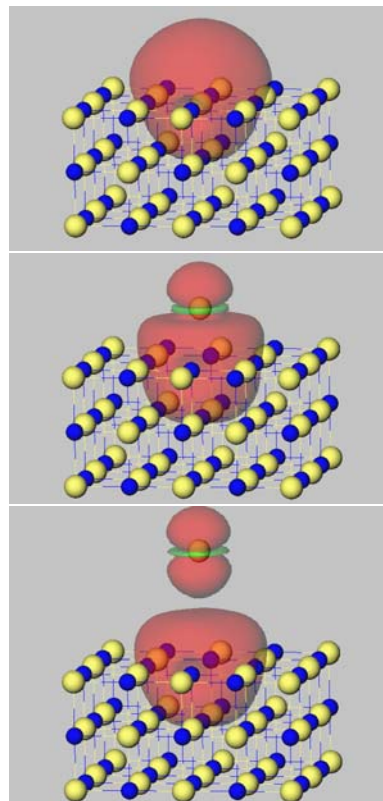
**Figure 1.** Velocity profiles  $I(^2P_{3/2})$  desorption from KI excited at 5.47 and 5.25 eV. The velocity profile is obtained by recording the relative iodine-atom yield as a function of delay between pump and probe lasers.

Figure 1 shows the velocity profiles for hyperthermal I atoms ejected from the surface of KI. Through selective use of the excitation energy, we use the peak velocity data to accurately determine the surface exciton energy. Using this new method, we predict the surface exciton energies for KI, KBr, KCl, and NaCl within  $\pm 0.15$  eV. Our data, the measured and calculated shifts of the surface exciton energies with respect to the bulk excitons, combined with the available electron energy-loss spectroscopy data for alkali fluorides demonstrate a universal linear correlation with the inverse inter-atomic distance in these materials. The results suggest that surface excitons exist in all alkali halides, and their excitation energies can be predicted from the known bulk exciton energies and the obtained correlation plot.

In conjunction with the experiments, we have conducted *ab initio* electronic structure calculations to understand the ejection mechanism. Figure 2 shows a time series of calculations during the ejection of a halide atom. One can clearly see that the surface exciton wavefunction (top panel) has a very different topology and is more delocalized at the surface than is typical for a bulk exciton. This finding explains the lower kinetic energy of the excited electron at the surface. The essential components of this mechanism have been confirmed in a series of experimental studies. These studies also suggest that surface excitons can be made selectively without inducing significant bulk excitation and can therefore be used to induce specific surface reactions in the absence of undesirable side reactions, such as bulk defect formation.

## Reference

Hess WP, AG Joly, KM Beck, PV Sushko, and AL Shluger. 2004. "Determination of Surface Exciton Energies by Velocity Resolved Atomic Desorption." *Surface Science* 564(1-3):62-70.



**Figure 2.** Time series (top to bottom) calculation of the electron density for an alkali halide system undergoing surface exciton-induced atomic desorption.

## Radiation-Induced Genomic Instability and Non-Targeted Bystander Effects Induced by the Electron Microbeam

MB Sowa<sup>(a,b)</sup> and WF Morgan<sup>(b)</sup>

(a) Pacific Northwest National Laboratory, Richland, Washington

(b) University of Maryland School of Medicine, Baltimore, Maryland

*Through studies of radiation-induced genomic instability in human cells, we seek to understand the mechanisms underlying the onset of the carcinogenesis.*

Ionizing radiation induces many forms of DNA damage, both directly by energy absorption and indirectly by producing highly reactive free radicals (Resat and Morgan 2004a). In recent years, it has become evident that radiation also induces delayed genomic instability, defined as an increased rate of genetic alterations in the genome of progeny of irradiated cells multiple generations after the initial insult. Delayed effects include chromosomal rearrangements and aberrations (chromosomal instability), micronuclei, gene mutations, microsatellite instability, changes in ploidy, and decreased plating efficiency. Many of these effects appear to be mediated by non-targeted effects occurring in cells that were not traversed by an ionizing particle.

Ionizing radiation initiates the instability phenotype either directly by hitting the target cell or indirectly via the secretion of soluble factors or cell-to-cell gap junction mediated communication from an irradiated cell to a nonirradiated cell (Figure 1). Once initiated, instability can manifest in the progeny of that cell during clonal expansion and is measured by multiple

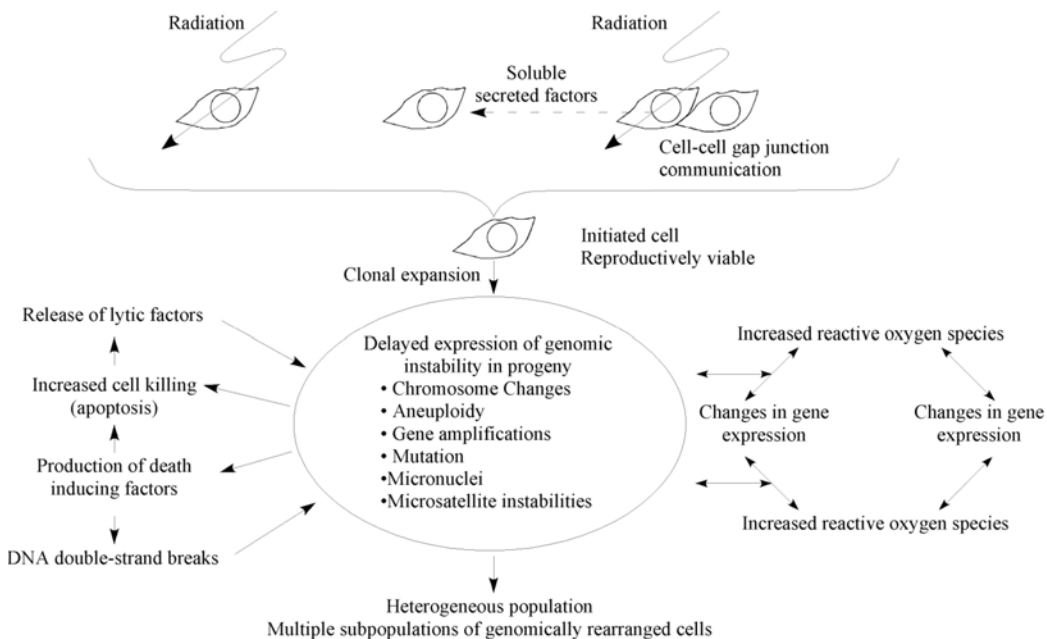


**Figure 1.** Schematic representation of radiation-induced genomic instability.

endpoints. Cell clones showing induced instability can also exhibit persistently elevated levels of reactive oxygen species, which in turn can stimulate changes in gene expression, and/or protein/enzyme levels. The combination of increased reactive oxygen species and subsequent altered cellular homeostasis provide protracted stimuli, perpetuating instability over time. Some unstable clones also generate soluble cytotoxic factors such that media from unstable clones is lethal when transferred to nonirradiated cells (Resat and Morgan 2004b). This death-inducing effect results in the induction of DNA double-strand cleavage rapidly after transfer to recipient cells leading to chromosome changes, micronuclei formation, and ultimately cell death. The majority of exposed cells die by apoptosis that might result in lytic products from these dead and dying cells contributing to the death-inducing effect and perpetuating instability over time. The end result is a heterogeneous population of cells containing multiple genomically rearranged subpopulations resulting from clonal expansion of a radiation-initiated cell. The phenotypes of radiation-induced genomic instability are similar to those described for tumor cells.

Investigating potentially rare events, such as induced instability occurring in cells that have survived exposure to ionizing radiation, demands an assay technique that can rapidly and reliably screen very large numbers of cells. We have developed such an assay that uses a green fluorescence protein (GFP)-based homologous recombination substrate. A plasmid vector, pCMV-EGFP2Xho, that carries two GFP direct repeats is linked to an SV40 promoter-driven *neo* gene. One copy of GFP, driven by a cytomegalovirus promoter, was inactivated by a +5 frame-shift mutation that created an *XhoI* site; the second copy had a wild-type coding sequence but lacked a promoter (Figure 2). This plasmid was transfected into human RKO cells (p53<sup>+/+</sup>).

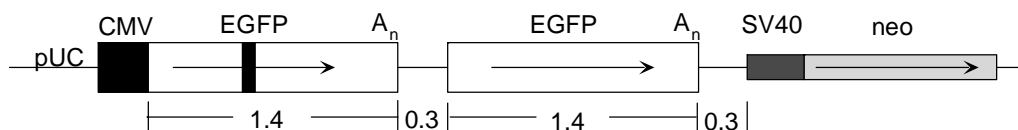


**Figure 2.** The plasmid vector pCMV-EGFP2Xho.

GFP<sup>-</sup> cells can be converted to GFP<sup>+</sup> directly by radiation-induced homologous recombination, in which case all cells within a colony would be GFP<sup>+</sup>. Similarly, pre-existing GFP<sup>+</sup> cells, if unchanged, will produce a GFP<sup>+</sup> colony, or they can be converted to GFP<sup>-</sup> by a variety of processes, including point mutagenesis, or induction of small- or large-scale deletions. These uniform GFP<sup>+</sup> or GFP<sup>-</sup> colonies reflect a stable GFP substrate. However, if radiation induces delayed instability at the GFP substrate, this will be reflected as mixed GFP<sup>+/-</sup> colonies.

We are currently using this GFP-based assay to investigate potential nontargeted, bystander-like effects as well as low-dose irradiation with the electron microbeam. We will compare induced instability as measured with the GFP reporter construct with our well-established baseline data for instability observed cytogenetically.

## References

Sowa Resat MB and WF Morgan. 2004a. "Microbeam Developments and Applications: A Low Linear Energy Transfer Perspective." *Cancer and Metastasis Reviews* 23(3-4):323-331.

Sowa Resat MB and WF Morgan. 2004b. "Radiation-Induced Genomic Instability: A Role for Secreted Soluble Factors in Communicating the Radiation Response to Non-Irradiated Cells." *Journal of Cellular Biochemistry* 92(5):1013-1019.

## Electron-Stimulated Reactions at the Interfaces of Amorphous Solid Water Films

GA Kimmel<sup>(a)</sup> and NG Petrik<sup>(a)</sup>

(a) Pacific Northwest National Laboratory, Richland, Washington

*The fundamental mechanisms of radiation damage to molecules in the condensed phase are of considerable interest to many fields, ranging from radiation biology to astrophysics. In particular, the structure of condensed water and its interactions with electrons, photons, and ions have been extensively studied and a variety of mechanisms for the non-thermal dissociation of water have been identified. However, the dynamics and kinetics of electronic excitations in water, that for example comprise biological systems, and their connection to the radiolysis products of water are still largely unknown.*

We have measured the electron-stimulated desorption (ESD) of D<sub>2</sub>, O<sub>2</sub>, and D<sub>2</sub>O; the electron-stimulated dissociation of D<sub>2</sub>O at the D<sub>2</sub>O/platinum interface; and the total electron-stimulated sputtering in thin D<sub>2</sub>O films adsorbed on platinum (111) as a function of the D<sub>2</sub>O coverage (i.e., film thickness) (Petrik and Kimmel 2004). Qualitatively different behavior is observed above and below a threshold coverage of approximately 2 monolayers (ML). For coverage less than approximately 2 ML electron irradiation results in D<sub>2</sub>O ESD and some D<sub>2</sub> ESD, but no detectable reactions at the water/platinum interface and no O<sub>2</sub> ESD. For larger coverage, electron-stimulated reactions at the water/platinum interface occur, O<sub>2</sub> is produced, and the total electron-stimulated sputtering of the film increases. An important step in the electron-stimulated reactions is the reaction between water ions (generated by the incident electrons) and electrons trapped in the water films to form dissociative neutral molecules. However, electron trapping depends sensitively on the water coverage. For coverage less than approximately 2 ML, the electrons trap preferentially at the water/vacuum interface, whereas for larger coverage, the electrons are trapped in the bulk of the film. We propose that the coverage dependence of the trapped electrons is responsible for the observed coverage dependence of the electron-stimulated reactions.

Figure 1 shows the D<sub>2</sub>O temperature-programmed desorption (TPD) spectra for amorphous D<sub>2</sub>O films with  $\theta = 1.0, 2.1,$  and  $3.0$  ML on platinum (111) for unirradiated films and after various irradiations with 87 eV electrons at 100 K. For all coverages, the energetic electrons cause desorption from the water film as seen in the loss of TPD intensity with increasing electron dose.

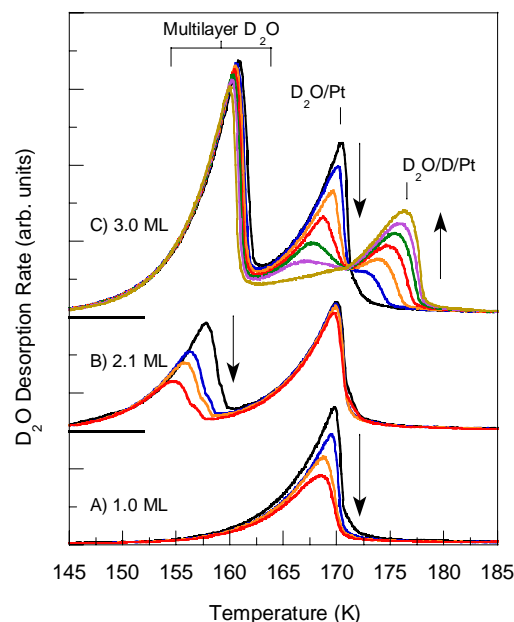


**Figure 1.** Post-irradiation TPD spectra for several electron fluences.

For  $\theta = 1.0$  and  $2.1$  ML, no other significant changes in the TPD spectra are seen (Figures 1A and B). However, for  $\theta = 3$  ML (Figure 1C), the behavior is qualitatively different. The desorption peak from the first adsorbate layer at approximately 170 K converts to a higher temperature peak at about 176 K with increasing electron fluence. There is a well-defined isosbestic point at approximately 171 K, indicating that the  $D_2O$  desorption is caused by two distinct species with overlapping TPD spectra. As the irradiation proceeds, the water molecules, which are initially bound to the clean platinum (111) surface, are converted to water interacting with D atoms adsorbed on the platinum (111) (*vide infra*). The data in Figure 1 suggest that a new electron-stimulated reaction channel becomes important between water coverage of 2 and 3 ML.

The high-temperature desorption feature in the post-irradiation TPD spectra for coverage greater than 2 ML (e.g., Figure 1C) is caused by water interacting with deuterium atoms adsorbed on the surface. Because  $D_2$  (or  $H_2$ ) dissociatively adsorbs on platinum (111), we compared the post-irradiation TPD spectra for  $\theta > 2$  ML with the TPD spectra for water on a deuterium pre-covered platinum (111) surface and found that they are essentially identical. The adsorbed deuterium recombinatively desorbs with second-order kinetics, and a clean platinum surface is recovered above about 340 K for both the irradiated films and the  $D_2$  pre-dosed films.

By comparing the post-irradiation water TPD spectra to TPD spectra from platinum (111) with a known coverage of D atoms,  $\theta_D$ , we can measure the number of D atoms deposited on the platinum (111) per incident electron per ML of water (Figure 2). The dissociation cross section has a threshold at about 2 ML and increases rapidly for  $2 \text{ ML} < \theta < 4 \text{ ML}$ . The ESD of  $O_2$ , and  $D_2$ , and the total sputtering versus coverage also have thresholds at approximately 2 ML.

Because of the strong coupling between adsorbate and substrate electronic wavefunctions, the platinum substrate might be expected to efficiently quench electronically excited molecules adsorbed on the surface, potentially explaining the low electron-stimulated reaction yields for  $\theta$  less than approximately 2 ML. However, we have previously shown that for thicker films, the electron-stimulated reactions leading to molecular hydrogen occur within about 2 ML of the water/platinum interface. Therefore, quenching of the electronically excited species involved in the reactions by the substrate is not the correct explanation for the observations. For coverages greater than 1 ML, the electronic structure of the adsorbed water should be independent of coverage. Therefore, changes in the ionization cross section of the adsorbed water molecules with coverage cannot explain the observations.

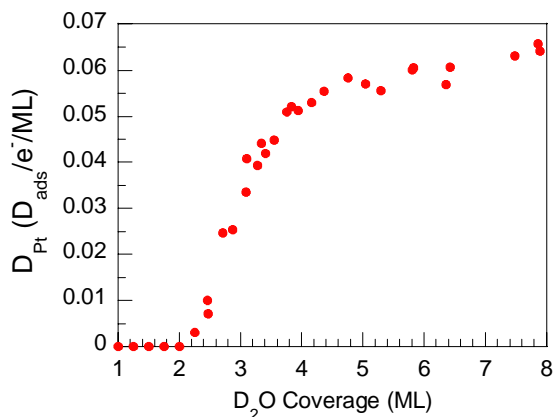


**Figure 2.** Number of D atoms deposited on the platinum (111) surface because of the electron-stimulated dissociation of  $D_2O$  per incident electron per ML versus the  $D_2O$  coverage.

In contrast, recent two-photon photoelectron spectroscopy measurements indicate that electron trapping is a sensitive function of the water coverage. For coverages less than 2 ML, the electrons are trapped at the vacuum interface, while for coverages greater than 3 ML, the electrons are trapped in the bulk of the water film. The electron-stimulated reactions observed in water films result primarily from dissociative, neutral excited states formed by electron-ion recombination. Therefore, the initial location and subsequent fate of these excited states depends on the thickness of the water film. For coverages less than 2 ML, the excited states are formed at the water/vacuum interface where the electrons trap and the subsequent reactions occur there (primarily water desorption). For coverages greater than 3 ML, electron-ion recombination occurs in the bulk of the water film. The neutral excited state (exciton) subsequently diffuses through the film and reacts when it reaches either the platinum/water or water/vacuum interfaces.

### Reference

Petrik NG and GA Kimmel. 2004. "Electron-Stimulated Reactions in Thin D<sub>2</sub>O Films on Pt(111) Mediated by Electron Trapping." *Journal of Chemical Physics* 121(8):3727-3735.

## Rotationally Resolved Infrared Spectroscopy and Absolute Infrared Cross Section Measurements of Methyl Nitrite

TA Blake,<sup>(a)</sup> LM Goss,<sup>(b)</sup> CD Mortensen,<sup>(b)</sup> SW Sharpe,<sup>(c)</sup> TJ Johnson,<sup>(c)</sup> and RL Sams<sup>(c)</sup>

(a) W.R. Wiley Environmental Molecular Sciences Laboratory, Richland, Washington

(b) Idaho State University, Pocatello, Idaho

(c) Pacific Northwest National Laboratory, Richland, Washington

No detailed information concerning the rotationally resolved infrared spectrum of methyl nitrite or its absolute absorption cross section existed prior to this study. Such information will be vital for detecting this molecule in the atmosphere and understanding its photochemistry as it reacts with air pollutants to form smog.

Methyl nitrite is formed in the atmosphere by the reaction of methoxy radicals with nitric oxide:

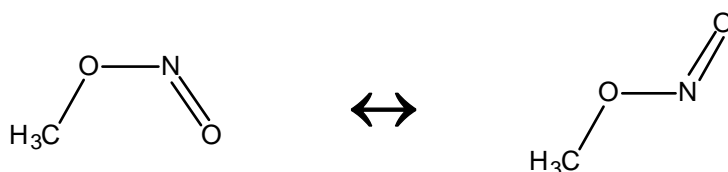


In daylight, it rapidly photolyzes in the near-ultraviolet region to re-form these radicals:



The formation of methyl nitrite is a nighttime sink for these radicals and can contribute to the aged-smog phenomenon in which pollutants from the previous day contribute to the photochemical air pollution on a particular day.

Methyl nitrite exists as a mixture of *cis* and *trans* rotational isomers, as shown in the reaction depicted below. Measurements of the *cis* ↔ *trans* equilibrium by <sup>1</sup>H nuclear magnetic resonance spectroscopy determined the thermodynamic parameters to be ΔH = 4.18 kJ/mol and ΔS = 9.62 J/mol K (Chauvel and True 1983).



This results in a ratio  $p_{\text{trans}}/p_{\text{cis}} = 0.59$  at 298 K and absorption bands of similar magnitude for the two isomers in the room-temperature, gas-phase infrared spectrum. Both of these isomers have *C<sub>s</sub>* symmetry and the 15 allowed fundamental vibrations include 10 of *A'* symmetry and 5 of *A''* symmetry.

Early microwave spectroscopy of methyl nitrite determined the rotational constants, barrier to internal rotation, dipole moment, and nuclear quadrupole coupling constants for both the *cis* and *trans* forms. Turner et al. (1979) determined complete structures for *cis*-methyl nitrite using microwave data from nine isotopic species and for *trans*-methyl nitrite using six

isotopic species. The *trans* isomer is a near-prolate rotor with an asymmetry parameter ( $\kappa$ ) value of -0.98 and a barrier to internal rotation of the methyl group of 29 cal/mol ( $10\text{ cm}^{-1}$ ). The *cis* isomer is an asymmetric top with  $\kappa = -0.75$  and a barrier to internal rotation of the methyl group of 2090 cal/mol ( $731\text{ cm}^{-1}$ ) (Turner et al. 1979). Further microwave measurements by Ghosh et al. (1980) extended the assignments for the *cis* form in the ground vibrational state to  $J = 20$  and observed transitions in excited states of the NO and  $\text{CH}_3$  torsions and the C–O–N deformation mode. They also determined centrifugal distortion, rotational, and quadrupole coupling constants and reported the barrier to internal rotation as  $734\text{ cm}^{-1}$ .

The infrared spectrum of methyl nitrite was first investigated by Tarte (1952), who determined that the doubling of the O–N=O bending, N–O stretching, and N=O stretching vibrations was caused by the existence of two rotational isomers. The vibrational assignments are reasonably well understood, and some work has been done using band contour simulations to predict band type but none of the mid-infrared work is rotationally resolved.

Using the high-resolution Fourier transform infrared spectrometer located at the W.R. Wiley Environmental Molecular Sciences Laboratory, we have recorded the first room-temperature, rotationally resolved mid-infrared band of *cis*-methyl nitrite (Figure 1) (Goss et al. 2004).

The  $\nu_8$  band is the N–O stretching mode that has  $A'$  symmetry and is expected to have *a*- and *b*-type rotational transitions. The  $\nu_8$  origin for the *cis* isomer is at  $841\text{ cm}^{-1}$  and the origin for the *trans* isomer is approximately  $28\text{ cm}^{-1}$  lower. These bands appear in an atmospheric window and would be suitable for remote sensing of this molecule. As described above, the barrier to internal rotation is much higher in the *cis* isomer than in the *trans* isomer; therefore, the spectrum is expected to be less congested for the *cis* isomer because of fewer resolved tunneling transitions.

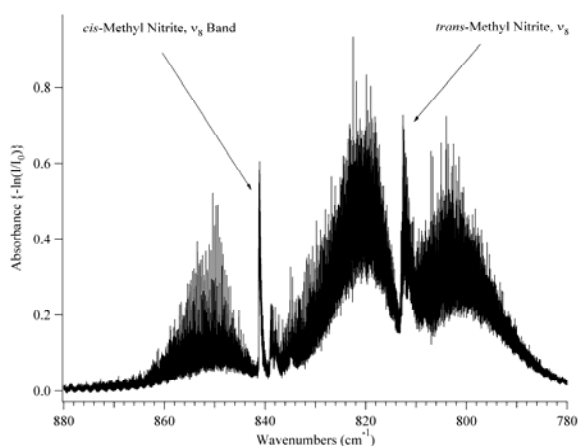


**Figure 1.** Methyl nitrite  $\nu_8$  band region showing absorptions from both the *cis* and *trans* isomers.

The  $\nu_8$  *cis* isomer band was recorded at a resolution of  $0.0015\text{ cm}^{-1}$ , and a total of 634 ro-vibrational transitions were assigned to the band. These lines and 32 microwave lines were globally fit to a Watson-type Hamiltonian with an root mean square deviation of  $0.00048\text{ cm}^{-1}$  (Figure 2). The fit provides improved ground state and  $\nu_8, v = 1$  rotational, centrifugal, and band origin constants. An additional 150 lines also were assigned but were not included in the fit because they were split by  $0.001$  to  $0.005\text{ cm}^{-1}$ , much larger than previously reported torsional or hyperfine splittings. The large size of the splittings can possibly be explained by the resonant interaction between the  $\nu_8$  and an excited torsional state. Several other mid-infrared bands have been recorded for both the *cis* and *trans* isomers. Assignment and fitting of these bands is proceeding.

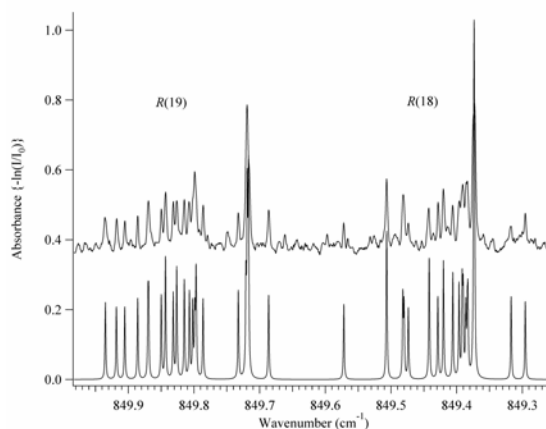


**Figure 2.** A portion of the  $\nu_8$  R(18) and R(19) regions for the *cis*-methyl nitrite isomer. The upper trace is from the experimental spectrum and the lower trace is from a simulation of the spectrum using the fit spectroscopic constants.

To make quantitative *in situ* atmospheric measurements of methyl nitrite, careful laboratory measurements of the molecule's absolute infrared absorption cross-section were made at Pacific Northwest National Laboratory as part of the Northwest Infrared Database (Sharpe et al. 2004). A minimum of six pressure path-length burdens at 5, 25, and  $50^\circ\text{C}$  each were measured using a benchtop Fourier transform spectrometer with a resolution of  $0.112\text{ cm}^{-1}$ . The sample pressures ranged from 1 to 32 Torr and were held in a 19.94-cm cell. Each methyl nitrite sample was pressurized to one atmosphere with dry nitrogen. A composite absolute absorbance spectrum normalized to a pressure path-length burden of 1 ppm-meter at 296 K is shown in Figure 3. Using this data, we can calculate individual absorption line strengths to the high-resolution infrared spectrum.

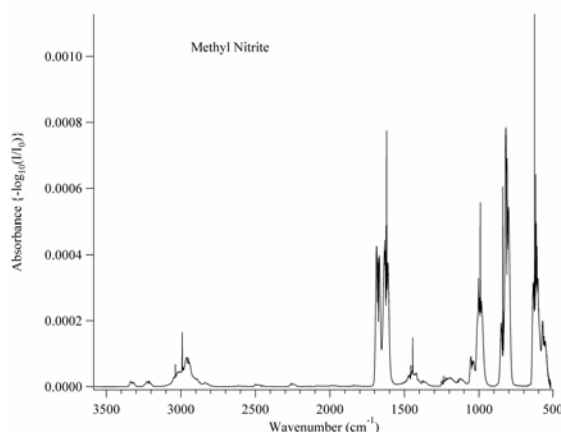


**Figure 3.** Infrared spectrum of methyl nitrite showing its absolute absorption cross section for a pressure path-length burden of 1 ppm-meter at 296 K.

## References

Chauvel JP and NS True. 1983. "Phase Effects on Conformational Equilibrium: Nuclear Magnetic Resonance Studies of Methyl Nitrite." *Journal of Physical Chemistry* 87(9):1622-1625.

Ghosh PN, A Bauder, and HH Gunthard. 1980. "Microwave Spectra of Ground and Excited Vibrational States of *cis*-Methyl Nitrite, CH<sub>3</sub>ONO." *Chemical Physics* 53(1-3):39-50.

Goss LM, CD Mortensen, and TA Blake. 2004. "Rotationally Resolved Spectroscopy of the  $\nu_8$  Band of *cis*-Methyl Nitrite." *Journal of Molecular Spectroscopy* 225(2):182-188.

Sharpe SW, TJ Johnson, RL Sams, PM Chu, GC Rhoderick, and PA Johnson. 2004. "Gas-Phase Databases for Quantitative Infrared Spectroscopy." *Applied Spectroscopy* 58(12):1452-1461.

Tarte P. 1952. "Rotational Isomerism as a General Property of Alkyl Nitrites." *Journal of Chemical Physics* 20(10):1570-1575.

Turner PH, MJ Corkill, and AP Cox. 1979. "Microwave Spectra and Structures of *cis*- and *trans*-Methyl Nitrite. Methyl Barrier in *trans*-Methyl Nitrite." *Journal of Physical Chemistry* 83(11):1473-1482.

## Toward the Solution Synthesis of the Tetrahedral Au<sub>20</sub> Cluster

HF Zhang,<sup>(a,b)</sup> M Stender,<sup>(a)</sup> R Zhang,<sup>(c)</sup> CM Wang,<sup>(c)</sup> J Li,<sup>(c)</sup> and LS Wang<sup>(a,b)</sup>

(a) Pacific Northwest National Laboratory, Richland, Washington

(b) Washington State University Tri-Cities, Richland, Washington

(c) W.R. Wiley Environmental Molecular Sciences Laboratory, Richland, Washington

*One of the long-standing objectives of cluster science is to discover highly stable clusters and use them as building blocks for bulk cluster-assembled materials, which may have dramatically different properties from their crystalline counterparts. This paper describes highly stable gold clusters that have potential for optical and catalytic research.*

The discovery of C<sub>60</sub> in the gas phase and its subsequent bulk synthesis provide classical inspiration and a prototypical example of highly stable clusters. However, it is generally believed that few other stable gaseous clusters may be assembled into bulk materials because of cluster-cluster interactions that lead to agglomeration. Indeed, no cluster-assembled materials have been synthesized on the basis of stable gaseous clusters other than the fullerenes, despite intensive experimental and theoretical efforts.

Recently, we reported that a 20-atom gold cluster possesses a tetrahedral (T<sub>d</sub>) structure with a remarkably large highest occupied molecular orbital-lowest unoccupied molecular orbital energy gap, suggesting that it would be highly inert chemically and may have novel optical and catalytic properties (Li et al. 2003).

Here, we report the observation of the tetrahedral Au<sub>20</sub> cluster in solution, ligated with triphenyl phosphine (PPh<sub>3</sub>) ligands, and its confirmation by theoretical calculations. This work represents a successful synthetic effort directly guided and motivated by a gas-phase observation, validating the gas-phase-to-condensed-phase approach for the discovery of cluster-assembled nanomaterials.

Because of potential cluster-cluster agglomeration, Au<sub>20</sub> must also be protected by ligands to be used as a building block for cluster-assembled materials. To maintain the unique structural and electronic properties of the T<sub>d</sub> Au<sub>20</sub>, the ligands must be carefully chosen. Thiol ligands strongly interact chemically with gold and would alter the electronic structure of the T<sub>d</sub> Au<sub>20</sub>. Preliminary theoretical calculations revealed that the Au<sub>20</sub>(PR<sub>3</sub>)<sub>4</sub> (R = H, Ph) complexes indeed possess high stability. The high-resolution transmission electron microscopy image in Figure 1 shows that the soluble samples contained gold nanoparticles with diameters as large as 3 nm, but the majority of the particles have diameters of less

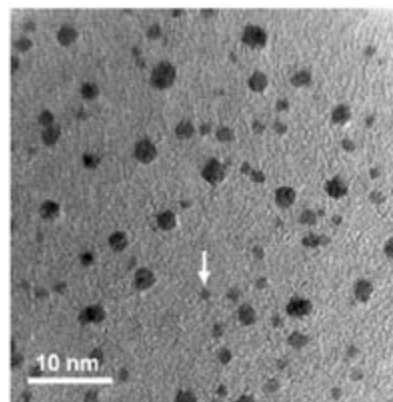


**Figure 1.** High-resolution transmission electron microscope image of synthesized Au-phosphine nanoparticles. The arrow points to one possible Au<sub>20</sub> cluster.

than 1 nm. The sample was further characterized using a high-resolution Fourier transform ion cyclotron resonance (FTICR) mass spectrometer that was accurately calibrated and equipped with an electrospray ionization source. A careful examination of the mass spectrum revealed doubly charged ions corresponding to  $\text{Au}_{20}$  clusters with eight and seven  $\text{PPh}_3$  ligands. To obtain structural information for the  $\text{Au}_{20}(\text{PPh}_3)_8^{2+}$  cluster, we conducted collision-induced dissociation experiments in the FTICR cell. These results, shown in Figure 2, suggest that the tetrahedral core of  $\text{Au}_{20}$  is intact in the  $\text{PPh}_3$ -coordinated clusters. This finding is consistent with our initial expectation and calculation that the four apex sites of  $\text{Au}_{20}$  are the most reactive sites that bind strongly to the four  $\text{PPh}_3$  ligands.

The current experimental and theoretical results suggest that  $T_d$   $\text{Au}_{20}$  clusters coordinated with phosphine ligands may be obtained in bulk quantity. It is expected that by increasing the size of the ligands, one can synthesize the  $T_d$   $\text{Au}_{20}$  clusters with only the four apex sites coordinated. These clusters may be promising catalysts with the highest surface area and well-defined surface sites.

These exciting results are featured in and on a recent cover of the *Journal of Physical Chemistry B* (Figure 3).

## Reference

Li J, X Li, HJ Zhai, and LS Wang. 2003. "Au<sub>20</sub>: A Tetrahedral Cluster." *Science* 299(5608):864-867.

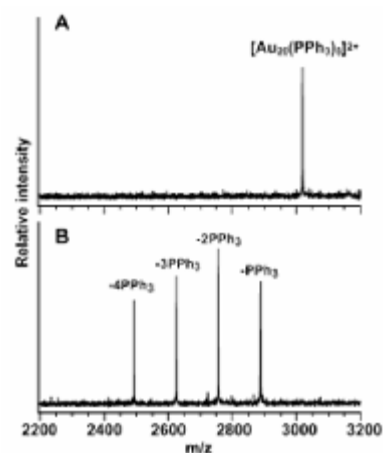


**Figure 2.** Collision-induced dissociation of  $\text{Au}_{20}(\text{PPh}_3)_8^{2+}$ .



**Figure 3.** Tetrahedral  $\text{Au}_{20}$  cluster shown on the cover of *Journal of Physical Chemistry*.

## Palladium Nanoclusters Supported on MgO(100): Effects of Cluster Size on Chemisorption Properties

*S Tait,<sup>(a)</sup> CT Campbell,<sup>(a)</sup> BD Kay,<sup>(b)</sup> and Z Dohnálek<sup>(b)</sup>*

*(a) University of Washington, Seattle, Washington*

*(b) Pacific Northwest National Laboratory, Richland, Washington*

*The study of atomic-scale interactions of adsorbed metals such as palladium on metal oxide surfaces is important in catalysis because the nature of these interactions determine catalytic activity. Examining such systems can lead to improvements in a wide range of industrial, environmental, and consumer applications, such the efficiency and cleanliness of chemical processes.*

Because of research on model catalyst systems during the last decade, much progress has been made in understanding supported metal catalysts at the nanometer scale. By studying these model systems, improvements in the efficiency and cleanliness of industrial chemical reactions can be accomplished. Understanding the effect that the nanometer-scale confinement of matter has on catalytic properties currently is a scientific challenge. Detailed analysis at the nanoscale allows us to probe the atomic-scale interactions of adsorbed metals and their oxide supports, both with each other and with other adsorbed species.

Nanometer-sized palladium particles supported on oxides are active catalysts for a variety of important reactions involving small alkanes. For example, low-temperature combustion of methane allows cleaner energy production because it minimizes NO<sub>x</sub> pollution. The intent of this project is to study adsorption of small alkane molecules on MgO(100) and the effects of particle size on the adsorption and dissociation of methane on model catalysts consisting of size-controlled palladium nanoclusters supported on MgO(100).

This work has been done using a sophisticated molecular beam surface scattering apparatus in the W.R. Wiley Environmental Molecular Sciences Laboratory at Pacific Northwest National Laboratory (Figure 1). This apparatus has a suite of surface science capabilities that are especially important for this project, including three quadruply pumped molecular beams, precise sample position control, precise control of beam angle of incidence on the sample, a quadrupole mass spectrometer (QMS) for background measurement, a line-of-sight QMS rotating about the sample, precise sample temperature control in the range 20 to 2000 K, Auger electron spectroscopy, x-ray photoelectron spectroscopy, metal vapor deposition sources, a quartz crystal microbalance, and computer-instrument interfacing for automated experiment control.

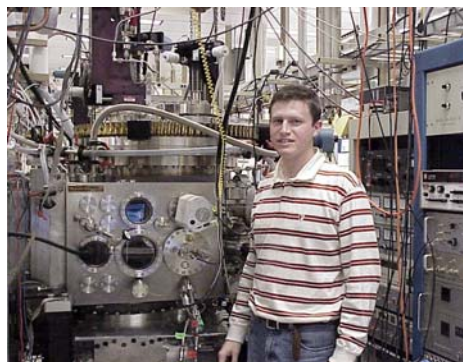
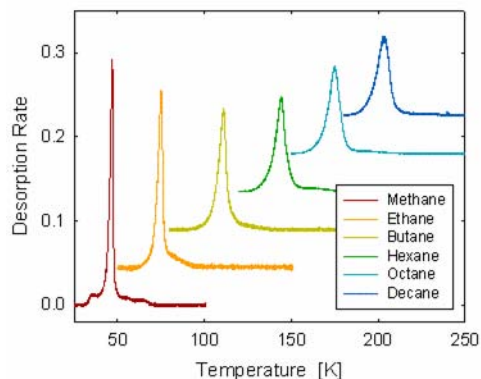


**Figure 1.** Graduate student from the University of Washington conducts research using the EMSL molecular beam scattering instrument.

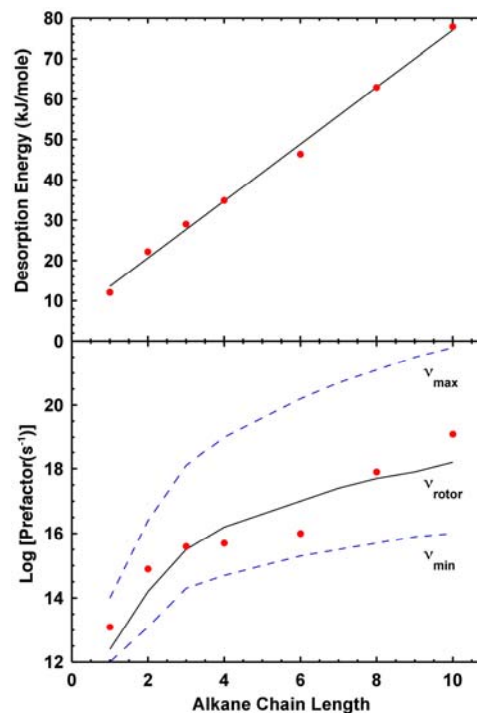
As part of our initial approach to address this problem, we used molecular beam scattering and temperature-programmed desorption (TPD) at low temperatures to study the adsorption and dissociation of hydrocarbons (methane, ethane, butane, hexane, octane, and decane) on MgO(100) thin films. Highly collimated molecular beams of the small alkane molecules are impinged on the sample. We see that the initial sticking probability increases with molecule size up to octane at which point the sticking coefficient is unity. As the size of the alkane molecule increases, there are more modes available to dissipate the incident kinetic energy of the molecule. The TPD experiments provide information about the adsorption energy of the alkane molecules on the MgO surface.

Figure 2 shows the TPD spectra for a series of small straight chain hydrocarbons from an epitaxially grown MgO(100) thin film. The hydrocarbons are deposited on the substrate at about 20 K, and each spectrum corresponds to one monolayer of the hydrocarbon on the MgO thin film. We observe a clear trend of increasing desorption energy with increasing alkane chain length. The spectra show that the TPD peak shifts to higher temperature with an increasing chain length that is consistent with an increase in binding energy with chain length.

Figure 3 shows the coverage-dependent desorption energy and desorption prefactor for a series of normal (straight chain) alkanes. These values are extracted from a TPD analysis technique that allows the coverage-dependent desorption energy to be accurately determined by mathematical inversion of a TPD spectrum, assuming only that the prefactor is coverage-independent. A variational method is used to determine the prefactor that minimizes the difference between a set of simulated TPD spectra and corresponding experimental data. The data show that the prefactor for desorption increases dramatically with chain length. The observed increase can be physically justified by considering the increase in rotational entropy



**Figure 2.** TPD spectra of a series of straight-chain hydrocarbons desorbing from an epitaxially grown MgO thin film. Each spectrum corresponds to one monolayer coverage of the given species.



**Figure 3.** Desorption energy (top graph) and desorption prefactor (bottom graph) for a series of normal chain alkanes. The lines indicate prefactors calculated using various rotation models.

available to the molecules in the gas-like transition state for desorption. The lines are predictions using various models to calculate the entropic change between a molecule adsorbed on the surface and one in the gas phase.

The next step in this research project is to study the dissociation of alkanes on MgO-supported palladium nanoparticles for several palladium coverages and beam energies. These measurements will advance our specific understanding of the catalytic activity of this important combustion catalyst and our general understanding of particle-size effects in hydrocarbon catalysis.

## Biological Applications of Imaging Micro- and Nanoscale Metal Oxides Using Multiphoton Microscopy

GR Holtom,<sup>(a)</sup> MF Romine,<sup>(b)</sup> and JS McLean<sup>(b)</sup>

(a) W.R. Wiley Environmental Molecular Sciences Laboratory, Richland, Washington

(b) Pacific Northwest National Laboratory, Richland, Washington

*Live-cell imaging is useful in the research of microorganisms that may be helpful bioremediators. Despite the vast research activity involving live-cell imaging using fluorescent material and continuing improvements in methods and instrumentation, a number of characteristic problems remain that limit the quality of three-dimensional images in long-duration imaging.*

Problems with live-cell imaging are fundamentally related to the physics of the organic chromophores usually employed. These problems appear as photo-bleaching or as photo-induced damage to the cells. We are investigating several technologies involving multiphoton microscopy methods to solve this problem, including coherent anti-Stokes Raman scattering (CARS) and two- and three-photon excitation of fluorescence. Metal oxides, in the form of submicron-size particles (i.e., on the microscale) or sub-100-nm particles (i.e., nanoscale), are resistant to photobleaching but require engineering to avoid particle aggregation. These nonfluorescent species require new nonlinear optical methods for detection, but several metal oxides, particularly several forms of iron oxide, may be produced biogenically and are important in bacterial growth.

We are particularly interested in biofilms and biological activity of *Shewanella oneidensis*, an organism capable of reducing metal oxides. This capability potentially could be used to stabilize toxic or radioactive soluble oxides in the aqueous subsurface, thereby rendering them insoluble and reducing their hazard. A number of imaging technologies with various resolutions can be used, but in general, there is a need for a high-sensitivity, high-resolution method that can be used to image live bacterial cultures. In Figure 1 we show the simultaneous imaging of unlabeled *S. oneidensis*, with the green channel showing an autofluorescent extracellular matrix and the red channel showing the bacteria by CARS imaging of the bacterial hydrocarbon. Optical images can be produced in closed optical cells to control oxygen levels with controlled flow and nutrient characteristics for long time durations. To investigate the local biological state of the bacteria, which varies with nutrient concentrations, we incorporate fluorescent protein markers linked to particular active genes. We also have developed

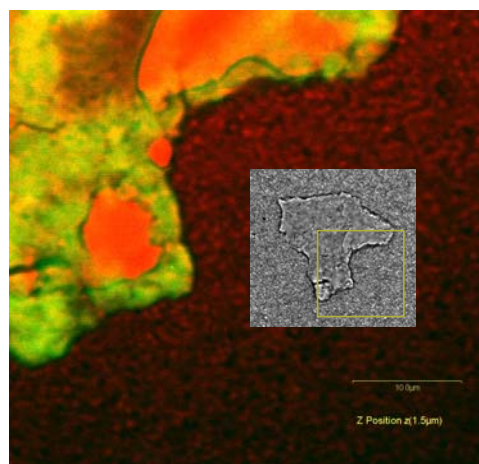


**Figure 1.** One slice of a three-dimensional multiphoton image set, showing CARS image (red) and two-photon excited fluorescence (green) of *S. oneidensis* MR-1 in a live biofilm. The bacteria are unstained, are visible in the CARS channel by their hydrocarbon content, and appear densely both within and outside the fluorescent matrix. The inset shows a larger area bright-field image of the biofilm matrix, which is attached to the cover slip of the flow cell. A wide, shallow biofilm surrounds the dense matrix region.

embedded nanoparticle sensors to probe the dissolved oxygen content, which is depleted by metabolic activity, and which affects biofilm structure and growth.

The materials science community has been interested in the nonlinear optical properties of iron oxides for at least the last decade, although the measurements involve detection techniques other than the CARS method (Hashimoto et al. 1996). The nonlinear optical susceptibility  $\chi^{(3)}$  is the largest of all inorganic oxides reported to date, although other metal oxides have properties that are useful and may be valuable for bioimaging.

Other metal oxides of interest are  $\text{TiO}_2$  and  $\text{ZnO}$ , an n-type semiconductor analogous to the II-VI materials used in quantum dots such as  $\text{CdS}$ . These oxides are used in large quantities commercially and are now being produced in nanoscale particles that have unknown environmental and health properties. Figure 2 shows high-contrast CARS images of  $\text{TiO}_2$  nanoparticles in macrophages. The dark features mark one or more individual particles and the lighter features mark the cellular outline.

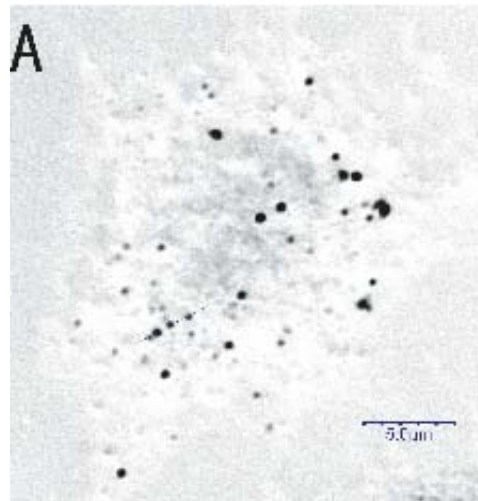


**Figure 2.** Simultaneous multichannel multiphoton images of a CARS image of a fixed macrophage cell after treatment with 50 nm  $\text{TiO}_2$  nanoparticles. The scale bar is 5 microns.

## Reference

Hashimoto T, T Yamada, and T Yoko. 1996. "Third-Order Nonlinear Optical Properties of Sol-Gel Derived  $\alpha\text{-Fe}_2\text{O}_3$ ,  $\gamma\text{-Fe}_2\text{O}_3$ , and  $\text{Fe}_3\text{O}_4$  Thin Films." *Journal of Applied Physics* 80(6):3184-3190.

## New Observations on the Up-Conversion Luminescence from CdTe Nanoparticles

W Chen,<sup>(a)</sup> AG Joly,<sup>(b)</sup> DE McCready,<sup>(b)</sup> J-O Malm,<sup>(c)</sup> and J-O Bovin<sup>(c)</sup>

(a) Nomadics, Inc., Stillwater, Oklahoma

(b) Pacific Northwest National Laboratory, Richland, Washington

(c) University of Lund, Lund, Sweden

*Up-conversion luminescence is luminescence in which the emitted wavelength is higher in energy than the excitation photons, in contrast to photoluminescence where the emitted wavelength is lower in energy than the excitation photons. Up-conversion luminescence has renewed interest in a number of novel applications, such as advanced biological imaging, low-energy panel displays, and three-dimensional microfabrication.*

Auger recombination, two-photon absorption, and thermally populated surface state absorption have been proposed to explain up-conversion luminescence (UCL). The Auger process involves transfer of energy from an excited electron-hole pair upon recombination to another electron or hole creating a highly excited carrier. This carrier is then available for recombination at a higher energy than the original excitation wavelength. Two-photon absorption may occur in one of two ways: the process may proceed through an intermediate state within the band gap and is then termed two-step two-photon absorption (TSTPA), or the process may proceed through a virtual intermediate state (TPA). The process occurring with a virtual intermediate state is significantly weaker and often requires higher excitation powers. Up-conversion via populated surface states involves thermally populated defect states that absorb a single photon and lead to higher energy luminescence. These processes show single-photon power dependences and a temperature dependence characterized by increasing UCL intensity at increasing temperatures. These processes are also extremely efficient, often only requiring a continuous-wave source, such as a He-Ne laser or a Xe lamp.

Figure 1 displays the photoluminescence and UCL spectra of three solid CdTe nanoparticle samples along with the absorption spectra of the solution samples from which the solid samples were precipitated. All three solutions have pronounced absorptions peaking at 522 nm, 563 nm, and 585 nm, which are blue-shifted from the energy gap of bulk CdTe at 827 nm because of quantum size confinement. Accordingly, the particle sizes are estimated to be approximately 3, 3.5, and 5 nm for the three samples.

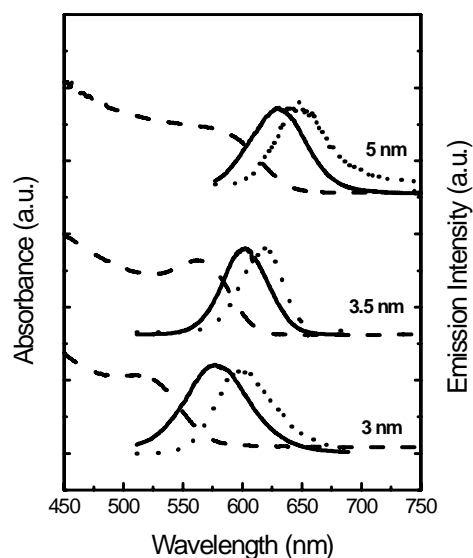


**Figure 1.** Optical absorption (dash), photoluminescence emission (solid), and up-conversion emission (dot) of the 3-nm, 3.5-nm, and 5-nm CdTe particle solid samples.

In the orange sample, the UCL maximum is about 16 nm red-shifted from that of the photoluminescence emission maximum. Similar results are observed for the yellow and red solid samples. For the yellow sample, the UCL is about 21.5 nm, and for the red solid sample, the up-conversion emission is about 17 nm red-shifted from that of the photoluminescence emission maximum.

Several publications have been dedicated to up-conversion from semiconductor nanoparticles; however, the mechanisms for UCL in semiconductor nanoparticles are still under debate. Often the dependence of UCL on input photon power dependence can yield some insight into the mechanism. The excitation laser power dependences of UCL intensity all display a roughly quadratic behavior both at room temperature and 10 K. Therefore, the UCL process is two-photon in nature, and thermally populated processes may be ruled out.

Both Auger and two-photon excitation processes may lead to a quadratic power dependence on the incident photon power. Auger-type up-conversion occurs most frequently in heterostructures or quantum well systems. This process requires that the incident photon energy span the band gap of at least one of the materials to form excitons in the smaller band-gap material. In the CdTe nanoparticles reported here, the incident photons are not energetic enough to produce electron-hole pairs or excitons. Therefore, Auger-type processes may be ruled out as a possible mechanism to explain the observed up-conversion, and it is reasonable to conclude that two-photon absorption is the dominant mechanism resulting in UCL in these samples.

The dramatic shift in the UCL spectra of the solid samples relative to the photoluminescence spectra argues that surface or defect states may be involved in the UCL process in the solid samples. Both one- and two-photon absorption (photoluminescence and UCL, respectively) ultimately result in identical final excitation energies; the fact that the UCL spectrum is red-shifted argues that different subsets of particles are excited in each case. For instance, surface or defect states of slightly lower energy than the band edge may be preferentially excited in the two-photon excited up-conversion relative to one-photon excitation because the excitation cross section to these states may be greater. This effect can be enhanced in the solid particles as the surface capping is of lower quality because of the removal of capping agents during precipitation in acetone. Therefore, the UCL may selectively excite the most defected particles within the sample. There is another possible cause of this red-shift in the UCL spectrum relative to the photoluminescence spectrum. The UCL may be composed of luminescence from slightly larger particles, which would show red-shifted luminescence. The two-photon excitation cross section to the larger particles may be slightly greater, which would result in the UCL selectively displaying this subset. Unfortunately, the experimental data does not allow a unique determination of the states involved in the up-conversion in this case.

## Single-Particle Studies of Atmospheric Aerosols

A Laskin,<sup>(a)</sup> JP Cowin,<sup>(b)</sup> and MJ Iedema<sup>(a)</sup>

(a) W.R. Wiley Environmental Molecular Sciences Laboratory, Richland, Washington

(b) Pacific Northwest National Laboratory, Richland, Washington

*The goals of this research are to characterize the chemical and physical properties of atmospheric aerosols and to establish quantitative relations between the composition of aerosols and their optical and hygroscopic properties, which are of primary importance to the effects of aerosol radiative forcing of earth's climate. Such data are used to build predictive models of local, regional, and global climatic impacts caused by natural and human-generated aerosols.*

The research involves collaboration with a number of university groups and the use of a suite of novel methodologies and state-of-the-art analytical techniques available in the W.R. Wiley Environmental Molecular Sciences Laboratory (EMSL). Specific goals of this research are to document the size and the chemical composition of specific aerosols along with their physical and chemical properties, elucidate the chemical and physical processes responsible for atmospheric evolution of specific types of aerosols, and document the effects of these processes on climate-related properties of evolving aerosols.

In a collaborative study with the group of V.H. Grassian (University of Iowa), we studied the chemistry of mineral dust particles reacting with  $\text{HNO}_3$ , a pervasive gas-phase species in polluted industrial areas. We demonstrated the complete laboratory processing of calcite particles (one of the most common minerals) and the subsequent formation of highly hygroscopic  $\text{Ca}(\text{NO}_3)_2$  (Figure 1). The resulting hygroscopic particles can act as efficient cloud condensation nuclei (CCN) in the earth's atmosphere. Under atmospheric conditions of relative humidity, processed  $\text{Ca}(\text{NO}_3)_2/\text{CaCO}_3$  particles absorb water efficiently and change their shape and size, hence changing the scattering and absorption efficiencies. This reaction, which is caused mostly by interaction of mineral dust with polluted air, can be a major chemical pathway for modifying mineral dust's properties in the atmosphere (Krueger et al. 2004; Laskin et al. 2004).

In a collaborative study with the group of B.J. Finlayson-Pitts (University of California, Irvine), we studied the hygroscopic properties of  $\text{NaNO}_3$  and mixed  $\text{NaCl}/\text{NaNO}_3$  particles

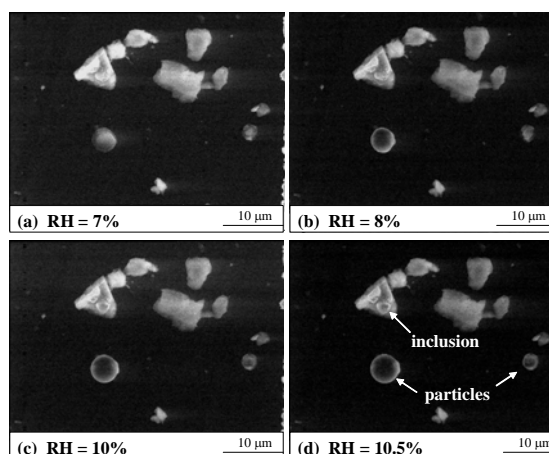


**Figure 1.** Environmental scanning electron microscope (ESEM) images of mineral dust particles reacted with  $14 \pm 1 \mu\text{Torr}$  of  $\text{HNO}_3$  and  $36 \pm 1\%$  relative humidity (RH) for 2 hours. The images are taken with increasing RH at  $T = 25^\circ\text{C}$ : (a) 7% RH, (b) 8% RH, (c) 10% RH, and (d) 10.5% RH. The presence of individual and internally mixed particles that undergo hygroscopic growth is evident. Adopted from Laskin et al. 2004.

using ESEM, a novel form of electron-probe based instrumentation. We showed that the hydration process of these particles does not exhibit a distinct deliquescence point, rather it shows continuous hygroscopic growth of particles typical for amorphous solids (Hoffman et al. 2004). The formation of unusual metastable, amorphous solid phases of  $\text{NaNO}_3$  and mixtures of  $\text{NaCl}$  with  $\text{NaNO}_3$  may play a significant role in both the chemistry and radiative properties of salt particles in the marine boundary layer and regions around dry lakes.

Other ongoing collaborative projects include aging of diesel exhaust particles with M.J. Molina and L.T. Molina (Massachusetts Institute of Technology), characterization and aging of biomass burning particles with W.C. Malm and J.L. Hand (National Park Service and Colorado State University, respectively), and characterization of mineral dust aerosols collected in the Mediterranean coastal area with Y. Rudich (Weizmann Institute, Israel).

## References

- Gaspar DJ, A Laskin, W Wang, SW Hunt, and BJ Finlayson-Pitts. 2004. "TOF-SIMS Analysis of Sea Salt Particles: Imaging and Depth Profiling in the Discovery of an Unrecognized Mechanism for pH Buffering." *Applied Surface Science* 231-2:520-523.
- Hoffman RC, A Laskin and BJ Finlayson-Pitts. 2004. "Sodium Nitrate Particles: Physical and Chemical Properties during Hydration and Dehydration, and Implications for Aged Sea Salt Aerosols." *Journal of Aerosol Science* 35(7):869-887.
- Krueger BJ, VH Grassian, JP Cowin, and A Laskin. 2004. "Heterogeneous Chemistry of Individual Mineral Dust Particles from Different Dust Source Regions: The Importance of Particle Mineralogy." *Atmospheric Environment* 38(36):6253-6261.
- Laskin J, KM Beck, JJ Hache, and JH Futrell. 2004. "Surface-Induced Dissociation of Ions Produced by Matrix-Assisted Laser Desorption/Ionization in a Fourier Transform Ion Cyclotron Resonance Mass Spectrometer." *Analytical Chemistry* 76(2):351-356.

## Soft-Landing of Peptide Ions on Self-Assembled Monolayer Surfaces

*J Alvarez,*<sup>(a)</sup> *RG Cooks,*<sup>(a)</sup> *JH Futrell,*<sup>(b)</sup> *SE Barlow,*<sup>(c)</sup> *and J Laskin*<sup>(b)</sup>

**(a) Purdue University, West Lafayette, Indiana**

**(b) Pacific Northwest National Laboratory, Richland, Washington**

**(c) W.R. Wiley Environmental Molecular Sciences Laboratory, Richland, Washington**

*It has been proposed that soft-landing of proteins could be used for generating protein microarrays. Similarly, peptide microarrays can be produced using soft-landing. Further, peptide ions present an ideal model system for studying the fundamental aspects of soft-landing of large ions on self-assembled monolayer surfaces. These are first steps in producing new surfaces suitable for use in sensors to selectively detect chemical and biological agents.*

Soft-landing of ions on surfaces (deposition of intact ions) is a process that occurs upon collision of low-energy ions (< 10 eV) with carefully selected semiconductive surfaces. Soft-landing experiments have been reported for small closed-shell ions (Miller et al. 1997), oligonucleotides (Feng et al. 1999), and most recently, for multiply protonated proteins (Ouyang et al. 2003). Most of these experiments used self-assembled monolayer (SAM) surfaces or liquid surfaces (Wu et al. 2000). SAM surfaces facilitate efficient dissipation of the initial kinetic energy of the ion, prevent ion neutralization by charge reduction or proton transfer, and minimize ion-molecule reactions on the surface.

Mass-selected peptide ions produced by electrospray ionization were deposited onto fluorinated self-assembled monolayer (FSAM) surfaces by soft-landing using a Fourier transform ion cyclotron resonance-mass spectrometer (FTICR-MS) specially designed for studying interactions of large ions with surfaces. Analysis of the modified surface was performed *in situ* by combining 2 keV Cs<sup>+</sup> secondary ion mass spectrometry with FTICR detection of the sputtered ions (FTICR-SIMS). Regardless of the initial charge state of the precursor ion, the SIMS mass spectra included a singly protonated peptide ion, peptide fragment ions, and peaks characteristic of the surface in all cases. In some experiments, multiply protonated peptide ions and [M+Au]<sup>+</sup> ions also were observed upon SIMS analysis of modified surfaces.

As previously reported for small organic ions, multiply charged peptide ions can retain charges (typically converting to singly charged ions) when deposited into selected organic monolayer surfaces such as SAM surfaces. The SAM surfaces are effective in reducing neutralization of the peptide ions by proton transfer. Charge retention of soft-landed ions was found to dramatically increase the ion yields obtained during SIMS analysis. We found that a significant number of soft-landed peptide ions retained their charge on the surface even after exposure to laboratory air, which allowed us to conduct *ex situ* characterization of modified surfaces using a time-of-flight (TOF)-SIMS instrument. The comparison of TOF-SIMS spectra obtained from an FSAM surface modified by soft-landing and a surface with the same amount of peptide deposited by electrospray provided further support for the presence of pre-formed ions on the former surface.

We further explored the effect of the initial kinetic energy of the ion on soft-landing. This was done by exposing the same surface to the ion beam of varying kinetic energy for the same time duration to eliminate possible variations between different surfaces. The buildup of the peptide signal was monitored as a function of time (Figure 1). If the kinetic energy had no effect on the amount of peptide that can be deposited onto an FSAM surface, we would expect to obtain a linear increase in signal as a function of time. The deviation from linearity of the plot shown in Figure 1a suggests that the efficiency of soft-landing decreases with collision energy. Indeed, the soft-landing efficiency obtained from the first derivative of the plot decreases with collision energy as shown in Figure 1b. This decrease can be rationalized by the corresponding decrease in the Langevin capture cross section shown as a solid line in the figure.

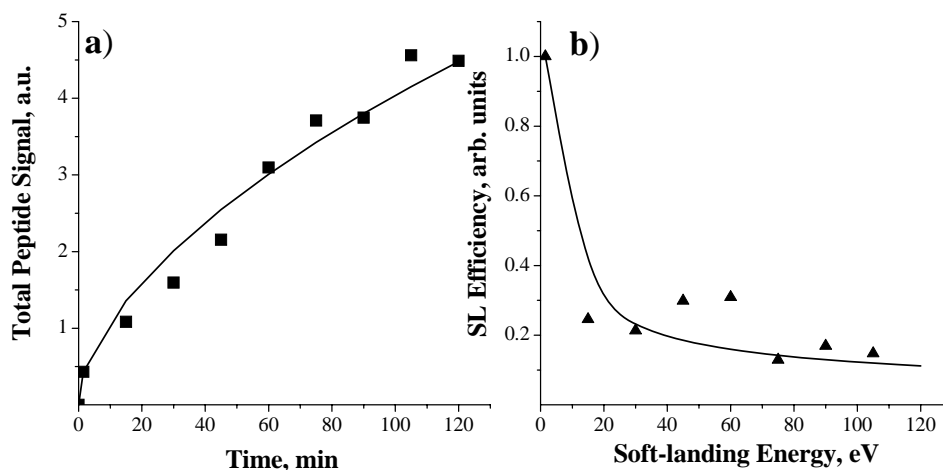


**Figure 1.** a) Cumulative peptide ion abundance (substance P) as a function of soft-landing energy. b) The efficiency of soft-landing. Lines are calculated from the capture cross-section at each collision energy.

## References

- Feng B, DS Wunschel, CD Masselon, L Pasa-Tolic, and RD Smith. 1999. "Retrieval of DNA Using Soft-Landing after Mass Analysis by ESI-FTICR for Enzymatic Manipulation." *Journal of the American Chemical Society* 121(38):8961-8962.
- Miller SA, H Luo, SJ Pachuta, and RG Cooks. 1997. "Soft-Landing of Polyatomic Ions at Fluorinated Self-Assembled Monolayer Surfaces." *Science* 275(5305):1447-1450.
- Ouyang Z, Z Takats, TA Blake, B Gologan, AJ Guymon, JM Wiseman, JC Oliver, VJ Davisson, and RG Cooks. 2003. "Preparing Protein Microarrays by Soft-Landing of Mass-Selected Ions." *Science* 301(5638):1351-1354.
- Wu K, MJ Jedema, and JP Cowin. 2000. "Ion Transport in Micelle-Like Films: Soft-Landed Ion Studies." *Langmuir* 16(9):4259-4265.

## Membrane Biology: Single-Molecule Fluorescence Imaging of Receptor Dynamics Identifies a Role for Cholesterol-Rich Membrane Domains

G Orr,<sup>(a)</sup> D Hu,<sup>(a)</sup> S Ozcelik,<sup>(a)</sup> L Opresko,<sup>(a)</sup> HS Wiley,<sup>(a)</sup> and SD Colson<sup>(a)</sup>

(a) Pacific Northwest National Laboratory, Richland, Washington

*The epidermal growth factor receptor is thought to be involved in breast cancer, and understanding its function may lead to insight into the biology of breast cancer and improved treatment of the disease. This research is aimed at elucidating the role of membrane microdomains in receptor function by focusing on real-time cellular behavior of individual receptors at the cell membrane and by developing and using cutting-edge imaging technologies.*

The flow of information through the epidermal growth factor receptor (EGFR) is shaped by molecular interactions in the plasma membrane (Figure 1). The EGFR is associated with membrane microdomains, or lipid rafts, but their role in modulating receptor mobility and subsequent interactions is unclear. To investigate the role of nanoscale rafts in EGFR dynamics, we used single-molecule fluorescence imaging to track individual EGFRs and their dimerization partner, EGFR 2 (HER2), in the membrane of human mammary epithelial cells (Figure 2). We found that the motion of both receptors was interrupted by dwellings within nanodomains. EGFR was significantly less mobile than HER2. This difference was likely due to filamentous proteins (F-actin) because their depolymerization led to similar diffusion patterns between the EGFR and HER2. Manipulations of membrane cholesterol content dramatically altered the diffusion pattern of both receptors. Cholesterol depletion led to almost complete confinement of the receptors, whereas cholesterol enrichment extended the boundaries of the restricted areas (Figure 3). Interestingly, F-actin depolymerization partially restored receptor mobility in cholesterol-depleted membranes. Our observations suggest that membrane cholesterol provides a dynamic environment that facilitates the free motion of EGFR and HER2, possibly by modulating the dynamic state of F-actin. The association of the receptors with lipid rafts could therefore promote their rapid interactions only upon ligand stimulation.

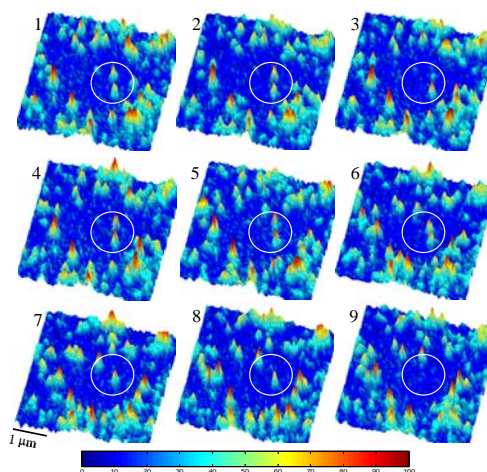


**Figure 1.** A series of consecutive images, taken at 130-ms intervals, showing individual AF-546-Fab fragment-tagged receptors as they entered a small photobleached area in the membrane of human mammary epithelial cells. Individual molecules were detected by their fluorescence blinking as shown in the third image (upper fluorescent spot within the circle), and by their single-step photobleaching as shown in the eighth image (upper spot), and the ninth image (lower spot).

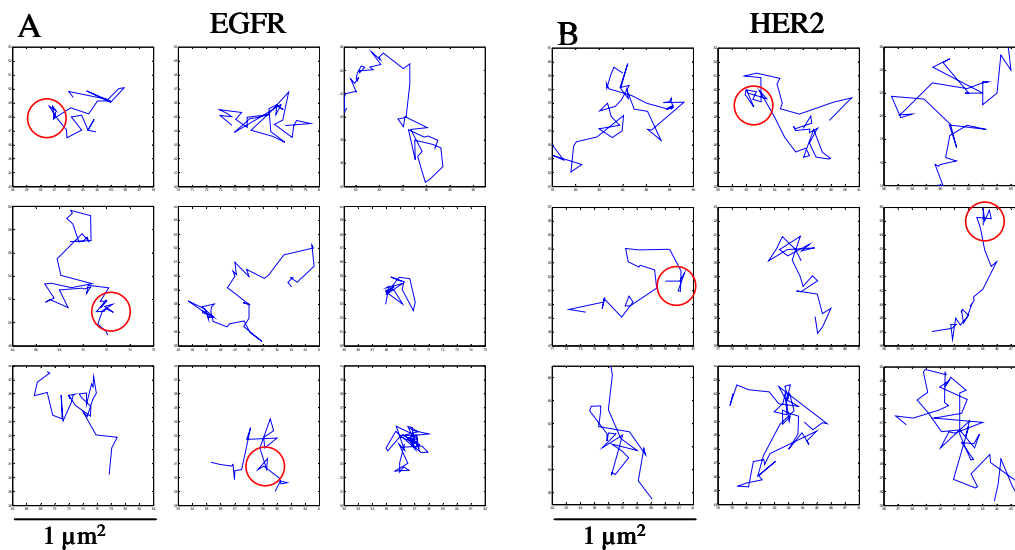


**Figure 2.** Traces of individual molecules show the receptors diffuse freely within larger microscale domains, interrupted by short confinement episodes within nanoscale domains. A: Typical traces of individual EGFR receptors showing their diffusion pattern in the plane of the membrane under normal conditions. The traces were taken in the lower membrane of the cell and are shown within  $1\text{-}\mu\text{m}^2$  ( $10 \times 10$  pixels) frames. Short dwellings within nanodomains are indicated by the red circles. B: The same pattern is observed by tracking individual HER2 molecules.

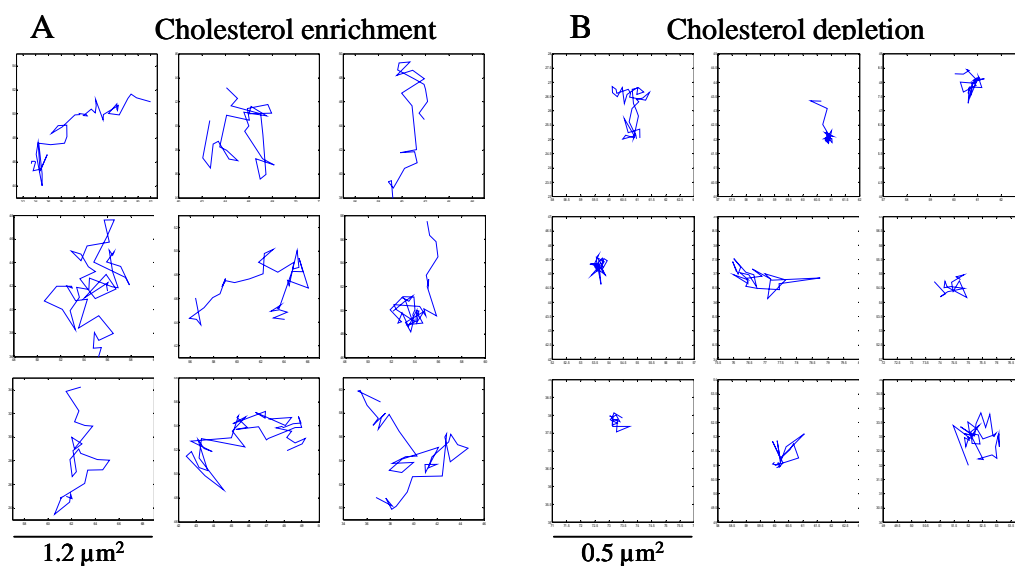


**Figure 3.** Manipulations of the cholesterol content of the membrane changed the pattern of the lateral motion of the receptors. A: Examples of EGFR traces in cholesterol-enriched membranes encased within  $1.2\text{-}\mu\text{m}^2$  boxes. The receptors covered, on average, larger areas than those covered under normal conditions. B: Traces of the receptors in cholesterol-depleted membranes, shown within  $0.5\text{-}\mu\text{m}^2$  boxes, were highly confined to nanoscale domains, with short and rare escapes.

The principal new finding to emerge from the research described in this paper is the role of membrane cholesterol in providing a dynamic environment that supports the lateral movement of EGFR and HER2 in the plane of the membrane. We propose a possible mechanism by which the modulation of receptor mobility could arise from F-actin polymerization underneath cholesterol-enriched lipid-rafts. We quantified the confined motion pattern of the two receptors and identified, by deviations from random-walk, dwellings within 50-nm domains that could indicate specific cellular interactions. The findings of this work also demonstrate that HER2 is more mobile in the plane of the membrane than EGFR, a difference that could result from the ability of EGFR to directly interact with F-actin. Because HER2 activation depends on its ability to form heterodimers with the EGFR, the presence of both receptors in cholesterol-enriched membrane domains might be an important aspect that regulates their activation upon ligand stimulation. Ligand stimulation is thought to induce formation of larger and more stable rafts that, in turn, could preserve the spatial information conveyed by the receptor through the membrane-associated signal transduction. The activation of EGFR has been shown to provide spatial and positional information during normal development or tumor invasion. The association of EGFR and HER2 with the lipid-raft network could therefore increase the reliability of the spatial information transduced by the receptors.

## Helium Diffusion through H<sub>2</sub>O and D<sub>2</sub>O Amorphous Ice: The First Observation of a Lattice Inverse Isotope Effect

JL Daschbach,<sup>(a)</sup> GK Schenter,<sup>(b)</sup> P Ayotte,<sup>(c)</sup> RS Smith,<sup>(b)</sup> and BD Kay<sup>(b)</sup>

(a) W.R. Wiley Environmental Molecular Sciences Laboratory, Richland, Washington

(b) Pacific Northwest National Laboratory, Richland, Washington

(c) University of Sherbrooke, Sherbrooke, Quebec, Canada

*Isotopic substitution has long been an invaluable tool in the experimentalist's arsenal for determining the microscopic details of a chemical reaction or diffusion. Normally, a heavier isotope reacts and diffuses more slowly than a lighter isotope. Researchers have uncovered that the diffusion rate of helium through amorphous solid water is the inverse of this behavior. This can lead to a more complete molecular-level assessment of water interactions within physical, chemical, and biological systems.*

In general, if a heavier isotope is substituted for an atom directly involved in a process, the rate for that process is usually slower. For example, in a reaction that involves the breaking of a bond containing a hydrogen atom, the substitution of deuterium will normally result in a decrease in the reaction rate. Thus, through a series of selective isotopic substitutions, one can learn about the microscopic details of a chemical reaction. The decrease in the rate is the result of a lower zero-point energy in the reactant well of the heavier isotope. A lowering of the zero-point energy means a larger energy barrier to reach the transition state and thus a lower rate.

Recently, researchers found that the diffusion rate of helium through amorphous solid water (ASW) is strongly dependent on the isotopic composition of the ASW lattice (Figure 1) (Daschbach et al. 2004). Further, the lattice isotope effect is the 'inverse' of a normal isotope effect, in that diffusion is faster in the heavier (D<sub>2</sub>O) isotope lattice. This is the first observation of an isotope effect for diffusion in a solid where the isotopic mass change occurs in the nominally static lattice. The explanation for this inverse isotope effect comes from transition state theory used to calculate the diffusion rate of helium between the ice-like cages. While the helium/D<sub>2</sub>O system lattice does have a lower zero-point energy in the reactant well (helium in an ice-like cage), there is a greater lowering of the zero-point energy at the transition state (helium in a hexagonal water ring), and the net result is an overall lower barrier for helium diffusion in D<sub>2</sub>O than in H<sub>2</sub>O. This effect, termed a 'tight' transition state, is well known for the inverse primary isotope effect observed in hydrogen/deuterium diffusion in palladium and in crystalline ice (Figure 2).

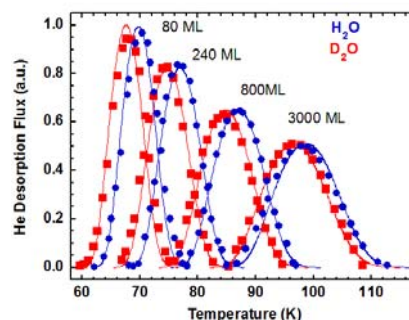


**Figure 1.** The temperature-programmed desorption (TPD) of helium-implanted ASW (H<sub>2</sub>O (circles) and D<sub>2</sub>O (squares) capped with 80, 240, 800, and 2400 monolayers of ASW. The lines through the data are Arrhenius fits using a kinetic hopping model. The data clearly show that helium diffuses more rapidly through D<sub>2</sub>O than H<sub>2</sub>O.

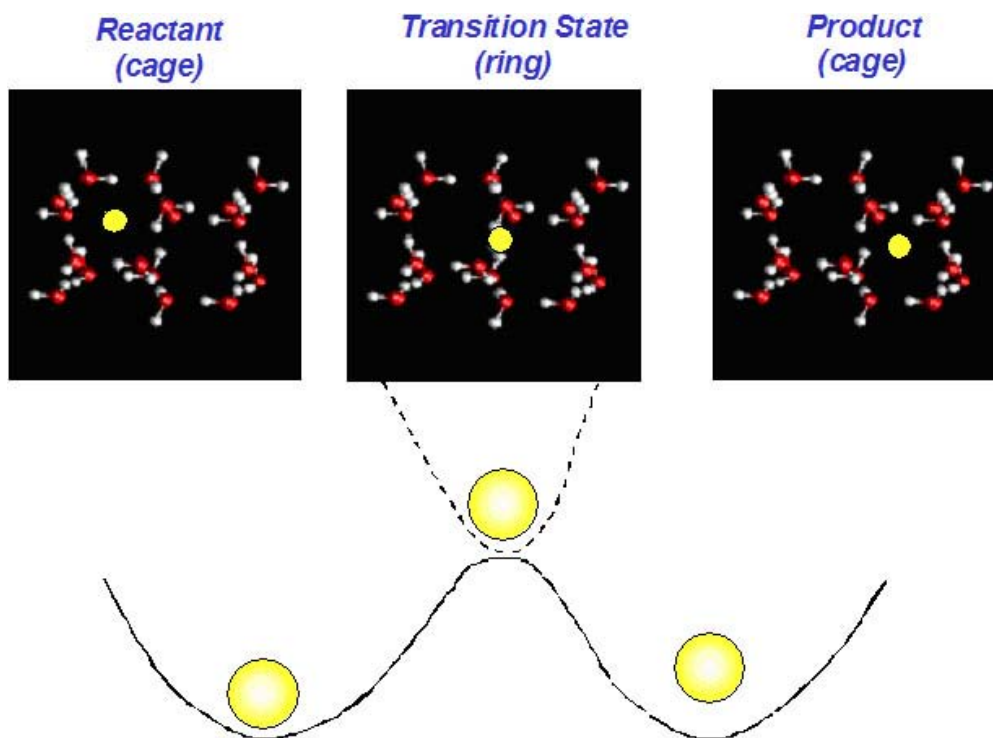


**Figure 2.** Helium diffusion model. Initially the helium atom is trapped in a water cage. To diffuse, it must overcome an energetic barrier (transition state). In this model, the transition state is a hexagonal water ring. After passing through the transition state, the helium atom drops into the adjacent water cage. The lattice inverse isotope effect observed for helium diffusion in  $\text{H}_2\text{O}$  and  $\text{D}_2\text{O}$  is the result of a 'tight' transition state.

In both of these cases, the isotope effect is caused by changes in the mass of the diffusing species. In the present case, the isotope effect arises predominantly from vibrational zero-point energy differences associated with the frustrated rotational modes of the  $\text{H}_2\text{O}$  ( $\text{D}_2\text{O}$ ) molecules comprising the water lattice. The magnitude of the secondary isotope effect is a sensitive probe of angular anisotropies in the helium-water interaction potential, and the experimental data provide an excellent test of the accuracy of the water/water and helium/water potentials.

### Reference

Daschbach JL, GK Schenter, P Ayotte, RS Smith, and BD Kay. 2004. "Helium Diffusion through  $\text{H}_2\text{O}$  and  $\text{D}_2\text{O}$  Amorphous Ice: Observation of a Lattice Inverse Isotope Effect." *Physical Review Letters* 92(19):198306.

## Surface-Induced Dissociation of Ions Produced by Matrix-Assisted Laser Desorption/Ionization in a Fourier Transform Ion Cyclotron Resonance Mass Spectrometer

*J Laskin,<sup>(a)</sup> KM Beck,<sup>(b)</sup> JJ Hache,<sup>(a)</sup> and JH Futrell<sup>(a)</sup>*

*(a) Pacific Northwest National Laboratory, Richland, Washington*

*(b) W.R. Wiley Environmental Molecular Sciences Laboratory, Richland, Washington*

*This work demonstrates an approach for obtaining a greatly improved sequence coverage for singly protonated ions using surface-induced dissociation in Fourier transform infrared cyclotron resonance mass spectrometry, which is particularly important for de novo sequencing of peptides and proteins. Ultra-high-resolution spectroscopy on the size and structure of large molecules is critical to deciphering the characteristics of biological molecules, polymers, and nanoparticles.*

Large molecules can be introduced into the gas phase using soft ionization techniques such as electrospray ionization or matrix-assisted laser desorption/ionization (MALDI) (Figure 1) and mass-analyzed using a variety of mass spectrometric approaches.

Although accurate mass measurement is an important prerequisite for mass spectrometric analysis of peptides and proteins, which is the focus of proteomics, it is not sufficient for unambiguous identification of these large molecules. For this reason, tandem mass spectrometry, based on structure-specific fragmentation of gas-phase ions, is a critical step for peptide and protein sequencing and identification. Because of the soft nature of electrospray ionization and MALDI, fragmentation of ions produced using these techniques requires a separate ion activation step in which the internal energy of the ion is increased by collisions with a neutral gas or with a surface, multiphoton absorption, or electron attachment. It is well established that dissociation of gas-phase peptides and proteins is a strong function of their charge state.

The combination of MALDI with Fourier transform ion cyclotron resonance (FTICR) mass spectrometry offers very high mass resolution and mass accuracy as well as multiple stages of tandem mass spectrometry that are essential for many applications. However, poor fragmentation patterns commonly obtained for MALDI ions using conventional ion activation techniques in FTICR mass spectrometry, such as sustained off-resonance irradiation (SORICID) or infrared multiphoton dissociation, limit the utility of this combination for structural characterization of biomolecules.

In this work, the utility of surface-induced dissociation (SID) is evaluated. These detailed studies of the kinetics and dynamics of SID of singly protonated ions (generated using electrospray ionization) in FTICR mass spectrometry revealed that at low collision energies, ion activation by collisions with surfaces closely mimics multiple-collision activation in the

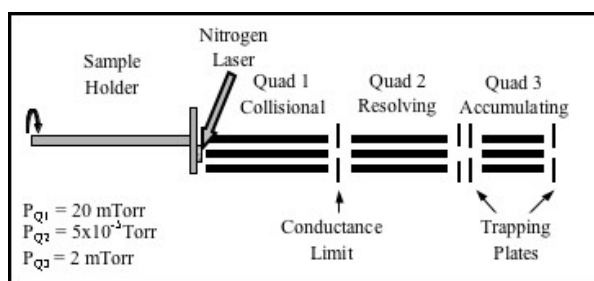


**Figure 1.** Schematic view of the intermediate-pressure MALDI source.

gas phase. A clear indication for this finding is the striking similarity between SORICID and low-energy SID spectra obtained for both small and large peptides. At high collision energies, we observed a transition in the dynamics of ion-surface interaction attributed to instantaneous dissociation of ions on the surfaces, shattering the transition. Shattering results in opening up a variety of dissociation pathways that cannot be achieved by slow activation methods. The shattering transition is particularly pronounced for arginine-containing peptides that fragment selectively at low collision energies.

The first results on SID of MALDI-generated ions in FTICR mass spectrometry demonstrated unique advantages of SID over SORICID for structural characterization of singly protonated peptide ions. As expected based on our prior experience, both slow activation by gas-phase collisions (SORICID) and fast excitation of ions by collisions with surfaces at relatively low collision energies provide similar fragmentation patterns. However, at higher collision energies, SID fragmentation of peptide ions is dominated by shattering, resulting in formation of a large number of sequence-specific fragment ions. Although the transition from recoil (slow decay) to shattering (fast decay) is a fairly sharp function of the internal energy of the ion, ion-surface impact results in deposition of a distribution of internal energies into the ensemble of ions that effectively mixes the slow and fast decay in the resulting SID spectrum (Figure 2).

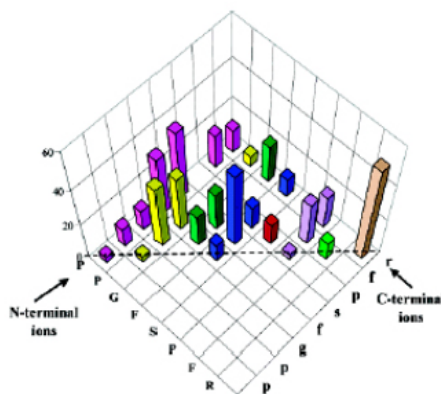


**Figure 2.** Backbone fragmentation map for the 55-eV SID of des-Arg1-bradykinin. The capital letters denote the N-terminal amino acid residue in the fragment ion sequence, and the lowercase letters correspond to the C-terminal amino acid residue.

This work took additional advantage of a wide internal energy distribution of ions resulting from collision with a stiff diamond surface, a process that provides a better mixing of slow and fast fragmentation channels. The SID results demonstrate a significantly better sequence coverage for singly protonated ions that are difficult to fragment using conventional ion activation techniques in FTICR mass spectrometry. It follows that the combination of SID with MALDI FTICR mass spectrometry is a new powerful method for characterization and identification of biomolecules. A full discussion of this work appears in Laskin et al. (2004).

## Reference

Laskin J, KM Beck, JJ Hache, and JH Futrell. 2004. "Surface-Induced Dissociation of Ions Produced by Matrix-Assisted Laser Desorption/Ionization in a Fourier Transform Ion Cyclotron Resonance Mass Spectrometer." *Analytical Chemistry* 76(2):351-356.

## User Projects

### **Low-Coordinated Oxygen Sites on MgO Surfaces**

*O Dimald, E Knozinger*

Vienna University of Technology, Vienna, Austria

### **High-Resolution, Gas-Phase Ultraviolet- and Infrared-Absorption Cross Sections of Naphthalene to Calibrate the First Differential Optical Absorption Spectroscopy Detection of Naphthalene in Mexico City**

*RM Volkamer, MJ Molina*

Massachusetts Institute of Technology, Cambridge, Massachusetts

### **Properties of Ice and Liquid Interfaces**

*JP Cowin, Y Lilach*

Pacific Northwest National Laboratory, Richland, Washington

### **Characterization of Quantum Cascade Lasers**

*TA Blake*

W.R. Wiley Environmental Molecular Sciences Laboratory, Richland, Washington

*MA Mangan*

Sandia National Laboratory, Albuquerque, New Mexico

### **Photoreflectivity in Ge/Si Thin Films**

*AG Joly*

Pacific Northwest National Laboratory, Richland, Washington

*D Brewe*

Argonne National Laboratory, Argonne, Illinois

*KM Beck*

W.R. Wiley Environmental Molecular Sciences Laboratory, Richland, Washington

*E Stern*

University of Washington, Seattle, Washington

### **Energetic Processes: Reactions in Thin Organic Films**

*GB Ellison*

University of Colorado, Boulder, Colorado

### **Theoretical Studies of Kinetic Processes in Nanoscale Ice Films**

*BD Kay, RS Smith, Z Dobnialek*

Pacific Northwest National Laboratory, Richland, Washington

*H Jonsson*

University of Washington, Seattle, Washington

### **Laser Ablation/Ionization Characterization of Solids**

*J Dickinson*

Washington State University, Pullman, Washington

**Vibration-Rotation Spectroscopy of Sulfur Trioxide***JW Nibler*

Oregon State University, Corvallis, Oregon

*A Masiello*

Pacific Northwest National Laboratory, Richland, Washington

*TA Blake*

W.R. Wiley Environmental Molecular Sciences Laboratory, Richland, Washington

*A Webber*

National Institute of Standards and Technology, Arlington, Virginia

*AG Maki*

Private Consultant, Mill Creek, Washington

**Aerosol Particle Generation, Collection, and Analysis***VN Mikebeev*

Innovatek, Inc., Richland, Washington

**Nanoparticle Fluorescence***W Chen*

Nomatics, Inc., Stillwater, Oklahoma

*AG Joly*

Pacific Northwest National Laboratory, Richland, Washington

**Laser-Induced Fluorescence Detection of C2 and C3 Vapor***RE Stevens*

Whitworth College, Spokane, Washington

**Photoelectron Spectroscopy of Group-VI Transition Metal Oxygen Clusters***T Waters, AG Wedd, RA O'Hair*

University of Melbourne, Melbourne, Victoria, Australia

**An Electrochemical Investigation into the Origin of the Enhanced Reactivity of Clays in Contact with Iron Metal***BA Balke*

Lewis and Clark College, Portland, Oregon

*JE Amonette*

Pacific Northwest National Laboratory, Richland, Washington

**Measurement of the Two-Photon Absorption Cross-Section of Natural Dyes***JN Woodford*

Eastern Oregon University, La Grande, Oregon

**Investigation of Hydrogen Tunneling in Tropolone***RL Redington*

Texas Technical University, Lubbock, Texas

**Material Characterization of Fluid-Loaded Lycopodium Membrane***JB Jones-Oliveira, CJ Bruckner-Lea*

Pacific Northwest National Laboratory, Richland, Washington

*SE Barlow*

W.R. Wiley Environmental Molecular Sciences Laboratory, Richland, Washington

**Kinetics in Ices with Complex Compositions***RS Smith*

Pacific Northwest National Laboratory, Richland, Washington

*P Ayotte*

University of Sherbrooke/Concordia University, Sherbrooke, Quebec, Canada

**Single Particle Laboratory Studies of Heterogeneous Reactions of Trace Atmospheric Gases with Particles Present in the Troposphere***VH Grassian, BJ Krueger*

University of Iowa, Iowa City, Iowa

*JP Cowin*

Pacific Northwest National Laboratory, Richland, Washington

*A Laskin*

W.R. Wiley Environmental Molecular Sciences Laboratory, Richland, Washington

**Resonant Surface Excitation of Potassium Salts by Selective Laser Desorption***MT Perozgo*

Mary Baldwin College, Staunton, Virginia

**Jet Spectrum of Nitromethane***DS Perry*

University of Akron, Akron, Ohio

**Measurement of Absolute Infrared Absorption Cross Sections of Nitric Acid***C Chackerian*

NASA Ames Research Center, Moffett Field, California

**High-Resolution Infrared Spectroscopy of Boron Trifluoride***AG Maki*

Private Consultant, Mill Creek, Washington

**Study of Nd<sup>3+</sup> Surface Adsorption on Calcite***SH Withers-Kirby*

University of Central Florida, Orlando, Florida

**Cellular Responses to Ionizing Radiation as Examined by FTIR***F Severcan*

Middle East Technical University, Ankara, Turkey

*MB Resat, BA Holben*

Pacific Northwest National Laboratory, Richland, Washington

**Size Resolved Chemical Composition of Automobile Generated Aerosol Via Single Particle Real-Time, Ion-Trap Mass Spectrometry***DG Imre, A Zelenyuk*

Pacific Northwest National Laboratory, Richland, Washington

**Spectroscopic Infrared Properties of Hydrogen Cyanide***MD Venkataraman*

College of William and Mary, Hampton, Virginia

**Scanning Mass Spectroscopy of Aerosols***GC Nieman*

Monmouth College, Monmouth, Illinois

**Photochemistry of a Diluted Magnetic Semiconductor Quantum Dot: A Possible Photocatalyst for Water Splitting***AG Joly*

Pacific Northwest National Laboratory, Richland, Washington

*DR Gamelin, KR Kittilstved*

University of Washington, Seattle, Washington

**High-Resolution Infrared Spectroscopy of Methyl Nitrite***LM Goss*

Idaho State University, Pocatello, Idaho

**Pd Nanoclusters Supported on MgO(100): Effects of Cluster Size on Chemisorption Properties***RS Smith, Z Dobnalek*

Pacific Northwest National Laboratory, Richland, Washington

*SL Tait, S Fain, CT Campbell*

University of Washington, Seattle, Washington

**Laboratory Studies of Atmospheric Processing of Sea Salt***BJ Finlayson-Pitts, JN Pitts, RC Hoffman*

University of California, Irvine, Irvine, California

**Development of an Electrospray Photoelectron Spectroscopy Apparatus with a Low-Temperature Ion Trap***LS Wang*

Washington State University Tri-Cities, Richland, Washington

**High-Resolution, Matrix-Assisted Laser Desorption/Ionization Imaging of Biological Samples***DS Wunschel*

Pacific Northwest National Laboratory, Richland, Washington

**High-Resolution Infrared Spectroscopy of Isotopically Substituted Butadienes***NC Craig*

Oberlin College, Oberlin, Ohio

**High-Resolution Infrared Spectroscopy of Acetaldehyde***JT Hougén*

National Institute of Standards and Technology, Gaithersburg, Maryland

**Investigation of the Electronic Structure of Fe-S Clusters***LS Wang*

Washington State University Tri-Cities, Richland, Washington

*CJ Pickett*

John Innes Centre, Norwich, United Kingdom

**Investigation of Zwitterions in the Gas Phase***SR Kass*

University of Minnesota, Minneapolis, Minnesota

*LS Wang*

Washington State University Tri-Cities, Richland, Washington

**Investigation of the Electronic Structure of Fe-S Clusters***T Ichibe, LS Wang*

Washington State University Tri-Cities, Richland, Washington

**Investigation of Aromatic and Other Novel Gas-Phase Atomic Clusters and Molecules***LS Wang, X Huang*

Washington State University Tri-Cities, Richland, Washington

*B Dai*

Pacific Northwest National Laboratory, Richland, Washington

*AI Boldyrev, BM Elliott, AN Alexandrova*

Utah State University, Logan, Utah

**Computational Chemistry Modeling of Main-Group and Transition-Metal Cluster Systems***LS Wang, K Boggavarapu, X Huang*

Washington State University Tri-Cities, Richland, Washington

*AN Alexandrova, BM Elliott*

Utah State University, Logan, Utah

*J Li*

W.R. Wiley Environmental Molecular Sciences Laboratory, Richland, Washington

**Single-Molecule Enzymatic Reaction Dynamics***HP Lu, D Hu*

Pacific Northwest National Laboratory, Richland, Washington

**Theoretical Models of the Adsorption and Desorption Dynamics in Compressed Monolayers**

*BD Kay, RS Smith, Z Dobnialek, GA Kimmel*

Pacific Northwest National Laboratory, Richland, Washington

*M Persson*

Chalmers/Goteborgs University, Goteborg, Sweden

**Adiabatic Following Spectroscopy Using Quantum Cascade Lasers**

*G Duxbury*

University of Strathclyde, Glasgow, United Kingdom

**Microscopic Studies of Hydration and Corrosion in Nuclear Materials Disposition**

*SA Joyce*

Los Alamos National Laboratory, Los Alamos, New Mexico

**Mexico City Municipal Area Air Pollution Study – 2003**

*ML Alexander, JP Cowin, BT Jobson, CE Lehner*

Pacific Northwest National Laboratory, Richland, Washington

*A Laskin*

W.R. Wiley Environmental Molecular Sciences Laboratory, Richland, Washington

*MJ Molina, L Molina, KS Johnson, BM Zuberi*

Massachusetts Institute of Technology, Cambridge, Massachusetts

**Surface Induced Dissociation of Peptides Using FTICR Mass Spectrometry**

*J Laskin, JH Futrell*

Pacific Northwest National Laboratory, Richland, Washington

*FM Fernandez*

Georgia Institute of Technology, Georgia Tech Research Corporation, Atlanta, Georgia

*K Kuppannan, VH Wjsocki, KA Herrmann*

University of Arizona, Tucson, Arizona

**High-Resolution Infrared Spectroscopy of Nitrogen Dioxide and Water**

*RL Sams*

Pacific Northwest National Laboratory, Richland, Washington

*TA Blake*

W.R. Wiley Environmental Molecular Sciences Laboratory, Richland, Washington

*MA Smith*

NASA Langley Research Center, Hampton, Virginia

**High-Resolution Infrared Spectroscopy of Methane**

*RL Sams*

Pacific Northwest National Laboratory, Richland, Washington

*TA Blake*

W.R. Wiley Environmental Molecular Sciences Laboratory, Richland, Washington

*L Brown*

Jet Propulsion Laboratory, Pasadena, California

**Measure the Anisotropy of a Membrane Protein at a Cell Membrane***HP Lu*

Pacific Northwest National Laboratory, Richland, Washington

*J Zheng*

University of Washington, Seattle, Washington

**Ultrasonic Catalysis of Chemical Reactions***KM Judd*

Pacific Northwest National Laboratory, Richland, Washington

*AM Williams*

Gonzaga University, Spokane, Washington

**Electron-Induced, Low-Dose Hypersensitivity***MB Resat*

Pacific Northwest National Laboratory, Richland, Washington

*GR Holtom*

W.R. Wiley Environmental Molecular Sciences Laboratory, Richland, Washington

*MC Joiner, B Marples*

Wayne State University, Detroit, Michigan

*BA Holben*

Washington State University, Pullman, Washington

*EJ Ashjian*

Southridge High School, Kennewick, Washington

**Electron-Induced Genomic Instability***MB Resat*

Pacific Northwest National Laboratory, Richland, Washington

*GR Holtom*

W.R. Wiley Environmental Molecular Sciences Laboratory, Richland, Washington

*WF Morgan, AR Snyder*

University of Maryland, Baltimore, Maryland

*BA Holben*

Washington State University, Pullman, Washington

*BJ Estes*

Gonzaga University, Spokane, Washington

*EJ Ashjian*

Southridge High School, Kennewick, Washington

**Triplet Decay Pathways of the Electrically Conducting Polymer***DM Laman, SW Miller*

Central Washington University, Ellensburg, Washington

*ZC Jacobson*

Wenatchee Valley College, Wenatchee, Washington

**Laser-Induced Neutral Metal Atom Desorption from Magnesium Oxide and Lithium Fluoride Probed Via Optical Spectroscopies***CN Afonso*

Institute of Optics, Madrid, Spain

**Single Molecule Dynamics of Protein DNA Interactions***JJ Han, AD Li*

Washington State University, Pullman, Washington

*HP Lu, R Liu*

Pacific Northwest National Laboratory, Richland, Washington

**Using the Environmental Scanning Electron Microscope for Studying the Atmospheric Transformations of Organic and Inorganic Particles***Y Rudich*

Weizmann Institute, Rehovot, Israel

**Fluorescence Imaging of Cellular Protein Dynamics***G Orr, SD Colson, D Hu*

Pacific Northwest National Laboratory, Richland, Washington

*GM Carr*

Brigham Young University, Provo, Utah

**Dissociative Charge Inversion of Peptides by Surface-Induced Dissociation***J Alvarez, RG Cooks*

Purdue University, West Lafayette, Indiana

*J Laskin, AK Shukla, JH Futrell*

Pacific Northwest National Laboratory, Richland, Washington

**Inelastic Electron Scattering Cross Section Measurements in Liquid Water***RG Tonkyn*

Pacific Northwest National Laboratory, Richland, Washington

*CM Brown*

Wadsworth Center, Albany, New York

**Dynamics Studies of Surface-Induced Dissociation of Polyatomic Ions***AK Shukla*

Pacific Northwest National Laboratory, Richland, Washington

*T Rezyat*

Office of Fellowship Programs, Santa Monica, California

**Fluorescence Microscopy of Cells and Particles***BJ Arthurs*

Washington State University, Pullman, Washington

*GR Holtom*

W.R. Wiley Environmental Molecular Sciences Laboratory, Richland, Washington

**Development of Data Analysis and Visualization Software – SpectraMiner***P Imrich, K Mueller*

State University of New York at Stony Brook, Stony Brook, New York

**Computer Programming of Data Acquisition Board for Single Particle Laser Ablation Time-of-Flight Mass Spectrometer (SPLAT-MS)***A Zelenyuk*

Pacific Northwest National Laboratory, Richland, Washington

*S Jambwalikar*

State University of New York at Stony Brook, Stony Brook, New York

**Signal Transmissions in Three-Dimensional Cell Structures***L Opresko, MB Resat*

Pacific Northwest National Laboratory, Richland, Washington

*BA Holben*

Washington State University, Pullman, Washington

**Determination of the Mo-X Bond Strengths in Oxomolybdenum Model Complexes***J Laskin*

Pacific Northwest National Laboratory, Richland, Washington

*P Basu, V Nemykin*

Duquesne University, Pittsburgh, Pennsylvania

**Dye Studies on CHO cells***MU Mayer-Cumblidge*

Pacific Northwest National Laboratory, Richland, Washington

**Ultrastructural Properties of Small Intestinal Submucosa***AD Janis, MC Hiles*

Cook Biotech Incorporated, West Lafayette, Indiana

**Laser-Materials Interactions: Theory and Experiment***AL Shtlger, PV Sushko*

London, University College, London, United Kingdom

*MH Engelhard*

W.R. Wiley Environmental Molecular Sciences Laboratory, Richland, Washington

**Single Particle Analysis of Smoke Aerosols during the Summer 2002: Yosemite Aerosol Characterization Study***JL Hand*

Colorado State University, Fort Collins, Colorado

**Second Harmonic Generation from Organic Water/Air Interfaces***AT Maccarone, GB Ellison*

University of Colorado, Boulder, Colorado

**Surface-Induced Dissociation of Polyatomic Ions***J Laskin, JH Futrell*

Pacific Northwest National Laboratory, Richland, Washington

**Single Molecule Approach for Understanding Epidermal Growth Factor Receptor Molecular Interactions***G Orr, HS Wiley, L Opresko, H Resat, D Hu, SD Colson, DJ Panther*

Pacific Northwest National Laboratory, Richland, Washington

*S Ozelik*

Ismir Institute of Technology, Urla, Turkey

**Electron Stimulated Reactions in Thin Water Films***GA Kimmel, NG Petrik*

Pacific Northwest National Laboratory, Richland, Washington

*AG Kavetski*

Khlopin Radium Institute, St. Petersburg, Russian Federation

**Condensed-Phase Chemical Physics of Low-Temperature Amorphous Solids and Gas-Surface Interactions***RS Smith, BD Kay, Z Dobnalek*

Pacific Northwest National Laboratory, Richland, Washington

**Use of Fluorimeter for Quantum Efficiency Studies on Semiconductor Quantum Dots***MG Warner, CJ Bruckner-Lea*

Pacific Northwest National Laboratory, Richland, Washington

**Single Molecule Electron Transfer Dynamics***HP Lu, VP Biju, D Hu*

Pacific Northwest National Laboratory, Richland, Washington

**Site-Specific Spectroscopy and Optical Imaging***HP Lu, D Pan*

Pacific Northwest National Laboratory, Richland, Washington

**Atomic Force Microscope-Enhanced Fluorescence Lifetime Imaging Microscopy and Raman Imaging***HP Lu, D Hu, D Pan, VP Biju*

Pacific Northwest National Laboratory, Richland, Washington

**Protein-Protein Interaction Dynamics***HP Lu, X Tan*

Pacific Northwest National Laboratory, Richland, Washington

**Microbial Cell Analysis and Imaging***HP Lu, VP Biju*

Pacific Northwest National Laboratory, Richland, Washington

**Ion Channel Protein Dynamics in Lipid Bilayer***HP Lu*

Pacific Northwest National Laboratory, Richland, Washington

*PK Kienker*

Yeshiva University, Albert Einstein College of Medicine, Bronx, New York

**A Variable Energy Electron Microbeam***MB Resat, GA Kimmel, BD Thrall*

Pacific Northwest National Laboratory, Richland, Washington

**Development of Multi-Functional Microscopy for Cancer and AIDS Research***TJ Weber, SD Colson*

Pacific Northwest National Laboratory, Richland, Washington

*GR Holtom*

W.R. Wiley Environmental Molecular Sciences Laboratory, Richland, Washington

*SJ Lockett, N Colburn, JM Wang, LG Rodriguez*

National Cancer Institute – Frederick, Frederick, Maryland

**Investigation of 4Fe-4S Cluster Complexes with Peptides as the Terminal Ligand***Y Fu, LS Wang*

Washington State University Tri-Cities, Richland, Washington

*J Laskin*

Pacific Northwest National Laboratory, Richland, Washington

**Atomically Resolved Studies of Transition Metal Oxides***RS Smith, Z Dobnalek*

Pacific Northwest National Laboratory, Richland, Washington

*JM White, O Bondarchuk*

University of Texas at Austin, Austin, Texas

**Chemical Characterization of Heterogeneous Inclusions in Soot Particles***H Wang, Z Yang*

University of Delaware, Newark, Delaware

**Temperature-Dependent Yield of Frenkel Pairs Generated by Valence Excitation in NaCl***K Tanimura*

Osaka University, Osaka, Japan

**Selective Immobilization of Biological Molecules on Single Walled Carbon Nanotube Surfaces***HP Lu, D Hu*

Pacific Northwest National Laboratory, Richland, Washington

*YD Sub*

Korea Research Institute of Chemical Technology, Yuseong-Ku DaeJeon, Republic of Korea

**EMSL CAT in Analytical Mass Spectrometry**

*RG Cooks*

Purdue University, West Lafayette, Indiana

*MV Johnston*

University of Delaware, Newark, Delaware

*LS Wang*

Washington State University Tri-Cities, Richland, Washington

*WL Hase*

Texas Technical University, Lubbock, Texas

*J Laskin, JH Futrell*

Pacific Northwest National Laboratory, Richland, Washington

*SE Barlow*

W.R. Wiley Environmental Molecular Sciences Laboratory, Richland, Washington

*P Basu*

Duquesne University, Pittsburgh, Pennsylvania

*FM Fernandez*

Georgia Institute of Technology, Georgia Tech Research Corporation, Atlanta, Georgia

*VH Wysocki*

University of Arizona, Tucson, Arizona

**Early Transition Metal Oxides as Catalysts: Chemical Physics**

*BD Kay, RS Smith, Z Dobnalek*

Pacific Northwest National Laboratory, Richland, Washington

**High-Resolution Infrared Spectroscopy of  $\text{BF}_2\text{OH}$** 

*J Fland*

University of Paris-South, Orsay Cedex, France

**High-Resolution Infrared Spectroscopy of Peroxynitric Acid**

*W Lafferty*

National Institute of Standards and Technology, Gaithersburg, Maryland

**Metal Sulfide Clusters in the Environment**

*MV Johnston, JM Spraggins*

University of Delaware, Newark, Delaware

*J Laskin*

Pacific Northwest National Laboratory, Richland, Washington

**Image Acquisition and Analysis of Fluorescent Biological Samples**

*BJ Arthurs*

Washington State University, Pullman, Washington

*GR Holtom*

W.R. Wiley Environmental Molecular Sciences Laboratory, Richland, Washington

**Photoelectron Spectroscopic Studies of Complex Anion Solvation in the Gas Phase**

*LS Wang, Y Fu, X Wang, X Yang, B Dai, H Lee, X Huang*

Washington State University Tri-Cities, Richland, Washington

**Phosphorous Poisoning of Automotive Catalysts**

*BG Bunting*

Oak Ridge National Laboratory, Knoxville, Tennessee

**Oxygen Desorption from Heavy Metal Oxides (Ge1)**

*KM Beck*

W.R. Wiley Environmental Molecular Sciences Laboratory, Richland, Washington

*OG Sanz, JD Gonzalo*

Institute of Optics, Madrid, Spain

**Charge Separation Kinetics in the  $\alpha$ -Cr<sub>2</sub>O<sub>3</sub>/ $\alpha$ -Fe<sub>2</sub>O<sub>3</sub> System**

*DM Laman*

Central Washington University, Ellensburg, Washington

**Photon-Stimulated Desorption of Cations from Ionic Solutions**

*JE Captain (Herring), TM Orlando*

Georgia Institute of Technology, Georgia Tech Research Corporation, Atlanta, Georgia

**Ultra-Trace Molecular Detection Instrumentation Based on Aerosol Nucleation with Rapid Preconcentration and Separation**

*VN Mikheev*

Innovatek, Inc., Richland, Washington

*N Laulainen, O Egorov*

Pacific Northwest National Laboratory, Richland, Washington

*SE Barlow*

W.R. Wiley Environmental Molecular Sciences Laboratory, Richland, Washington

**Development of Cell Permeable Dyes for *In Vivo* Live Cell Imaging**

*TC Squier, MU Mayer-Cumblidge, B Chen, L Shi*

Pacific Northwest National Laboratory, Richland, Washington

*GR Holtom*

W.R. Wiley Environmental Molecular Sciences Laboratory, Richland, Washington

**Analysis of Lipid Nanoparticle Interaction with Cell Membrane**

*HP Lu*

Pacific Northwest National Laboratory, Richland, Washington

*T Zhang*

National Institutes of Health, Bethesda, Maryland

## Staff

Roy E. Gephart, Manager, Technical Lead  
(509) 376-1421, roy.gephart@pnl.gov

Wayne P. Hess, Chief Scientist, Technical Lead (July 2003 – April 2004)  
(509) 376-9907, wayne.hess@pnl.gov

Christine C. Montgomery, Administrative Secretary  
(509) 376-9867, christine.montgomery@pnl.gov

Jayme Crow, Administrative Secretary (December 2002 – June 2004)  
(509) 376-2642, jayme.crow@pnl.gov

Stephan E. Barlow, Chief Scientist  
(509) 376-9051, se.barlow@pnl.gov

Kenneth M. Beck, Senior Research Scientist  
(509) 376-9152, kenneth.beck@pnl.gov

Thomas A. Blake, Senior Research Scientist  
(509) 376-8974, ta.blake@pnl.gov

John L. Daschbach, Senior Research Scientist  
(509) 376-2467, john.daschbach@pnl.gov

Gary R. Holtom, Chief Scientist  
(509) 376-5331, gary.holtom@pnl.gov

Martin J. Iedema, Senior Research Scientist  
(509) 376-6039, martin.iedema@pnl.gov

Alexander Laskin, Senior Research Scientist  
(509) 376-8741, alexander.laskin@pnl.gov

Marianne B. Sowa Resat, Senior Research Scientist  
(509) 376-9104, marianne.sowa-resat@pnl.gov

## Matrixed Staff

Alan G. Joly, Senior Research Scientist  
(509) 376-7707, agjoly@pnl.gov